Regulation of RhoA by STAT3 coordinates glial scar formation

Francois Renault-Mihara,[1] Masahiko Mukaino,[2] Munehisa Shinozaki,[1] Hiromi Kumamaru,[4] Satoshi Kawase,[1] Matthieu Baudoux,[1] Toshiki Ishibashi,[1,3] Soya Kawabata,[3] Yuichiro Nishiyama,[3] Keiko Sugai,[3] Kaori Yasutake,[3] Seiji Okada,[5] Masaya Nakamura,[3] and Hideyuki Okano[1]

[1]Department of Physiology, [2]Department of Rehabilitation Medicine, and [3]Department of Orthopedic Surgery, Keio University School of Medicine, Shinjuku-ku, Tokyo, Japan
[4]Department of Orthopedic Surgery and [5]Department of Advanced Medical Initiatives, Graduate School of Medical Sciences, Kyushu University, Fukuoka, Japan

Understanding how the transcription factor signal transducer and activator of transcription–3 (STAT3) controls glial scar formation may have important clinical implications. We show that astrocytic STAT3 is associated with greater amounts of secreted MMP2, a crucial protease in scar formation. Moreover, we report that STAT3 inhibits the small GTPase RhoA and thereby controls actomyosin tonus, adhesion turnover, and migration of reactive astrocytes, as well as corralling of leukocytes in vitro. The inhibition of RhoA by STAT3 involves ezrin, the phosphorylation of which is reduced in STAT3-CKO astrocytes. Reduction of phosphatase and tensin homologue (PTEN) levels in STAT3-CKO rescues reactive astrocytes dynamics in vitro. By specific targeting of lesion-proximal, reactive astrocytes in *Nestin-Cre* mice, we show that reduction of PTEN rescues glial scar formation in *Nestin-Stat3*$^{+/-}$ mice. These findings reveal novel intracellular signaling mechanisms underlying the contribution of reactive astrocyte dynamics to glial scar formation.

Introduction

Scarring is a general tissue response after injury, which separates injured areas from healthy tissue and promotes wound healing. In response to various central nervous system (CNS) insults, lesion-proximal, reactive astrocytes form a glial scar, working in concert with secreted molecules found in the lesion (Burda et al., 2016). Seclusion of the injured area limits tissue damage, restricts inflammation, and preserves function in the subacute phase of CNS injuries (Okada et al., 2006; Sofroniew, 2015). The long-standing view that glial scars hinder further axonal regeneration after CNS injury was recently challenged by a study showing that glial scars can support axon outgrowth, even in chronic spinal cord injuries (Anderson et al., 2016). These studies underscore the clinical relevance of a better understanding of the cellular and molecular mechanisms involved in glial scar formation.

Signal transducer and activator of transcription–3 (STAT3) has been identified as a key factor in astrogliosis (Ceyzériat et al., 2016). Specific ablation of STAT3 in reactive astrocytes is associated with defective glial scars, deficient lesion seclusion, enhanced demyelination, and increased neuronal losses after spinal cord injury (SCI) in mice (Okada et al., 2006; Herrmann et al., 2008). However, although the seclusion of the various nonneural cells that invade lesion centers has been shown to rely on STAT3-dependent reorientation of astrocytic processes (Wanner et al., 2013), the molecular mechanisms underlying the effect of STAT3 remains unknown. In the present study, we focused on the molecular mechanisms by which reactive astrocytes form glial scars and the molecular effectors of STAT3 in reactive astrocytes dynamics.

Results

STAT3 signaling promotes astrocyte migration in vitro (Okada et al., 2006) and promotes the seclusion of contusive spinal cord lesions by reactive astrocytes (Okada et al., 2006; Herrmann et al., 2008), but the underlying molecular mechanisms remain unclear. We sought to elucidate the role of STAT3 in controlling reactive astrocytes dynamics during glial scar formation by a classical migration study approach.

Correspondence to Francois Renault-Mihara: frenaultpro@yahoo.fr; Hideyuki Okano: hidokano@a2.keio.jp

Abbreviations used: CNS, central nervous system; dpi, days postinjury; ERM, ezrin, radixin, and moesin; FA, focal adhesion; GAP, GTPase-activating protein; GEF, guanine nucleotide exchange factor; IR, immunoreactivity; KO, knockout; LIF, leukemia inhibitory factor; LPA, lysophosphatidic acid; MLC2, myosin light chain-2; MMP2, matrix metallopeptidase-2; Nes-CCE, NestinCre/CAG-CAT-EGFP; PTEN, phosphatase and tensin homologue; ROCK, RhoA effector kinase; SCI, spinal cord injury; SOCS3, suppressor of cytokine signalling-3; STAT3, signal transducer and activator of transcription-3.

The Rockefeller University Press
J. Cell Biol. Vol. 216 No. 8 2533–2550
https://doi.org/10.1083/jcb.201610102

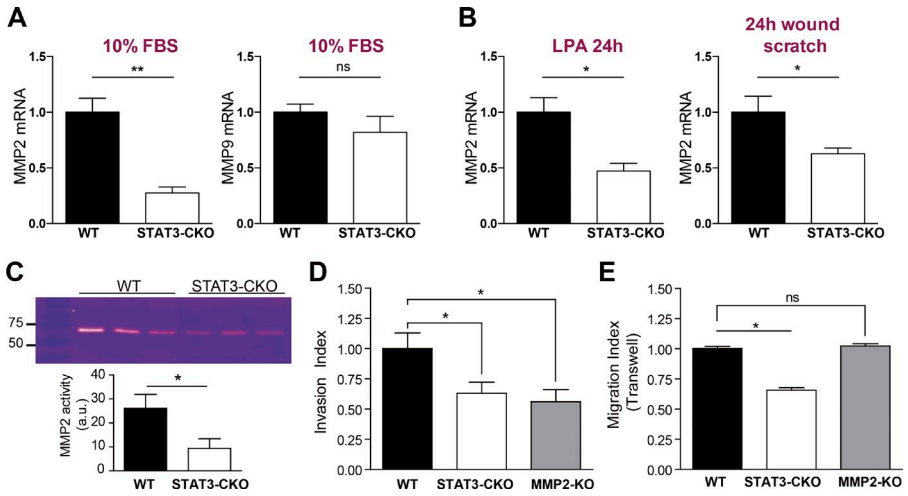

Figure 1. **MMP2 is an effector of STAT3 exclusively during the proteolytic migration of astrocytes.** (A) Real-time quantitative PCR analysis show that MMP2 mRNA is significantly reduced in STAT3-CKO astrocytes in usual culture conditions, whereas MMP9 is unchanged. Normalization is made with GAPDH, Mann-Whitney *U* test, $n = 5$ per group; **, $P < 0.005$. (B) MMP2 mRNA is also significantly lower in STAT3-CKO astrocytes versus WT astrocytes after challenge with LPA or wound scratch. (Normalization is made with GAPDH, Mann-Whitney *U* test, $n = 5$ per group). (C) Gelatin zymography of medium conditioned by astrocytes indicates significantly reduced secretion of MMP2 by STAT3-CKO astrocytes when compared with WT astrocytes (Mann-Whitney *U* test, $n = 3$). (D) STAT3-CKO astrocytes exhibit defective invasion through Matrigel, and reduced invasion of MMP2-KO astrocytes confirmed that MMP2 is necessary for invasion through Matrigel. (E) In contrast with STAT3-CKO astrocytes, MMP2-KO astrocytes do not show any significant reduction in migration in a trans-well assay compared with WT astrocytes, indicating that MMP2 does not affect nonproteolytic migration in this assay and suggesting the existence of other effectors of STAT3 involved in the nonproteolytic migration of astrocytes. *, $P < 0.05$; ns, not significant. Error bars indicate ±SEM.

Regulation of MMP2 by STAT3 exclusively affects the proteolytic migration of astrocytes

We first sought to determine whether matrix metallopeptidase-2 (MMP2), a major protease involved in tissue remodeling and a direct transcriptional target of STAT3 (Xie et al., 2004), is controlled by STAT3 in astrocytes. Real-time quantitative PCR analyses showed that the expression level of MMP2 was significantly reduced in astrocytes prepared from conditional knockout (KO) mice *Nestin-Stat3*$^{-/-}$ (STAT3-CKO astrocytes) compared with WT mice, grown in the usual culture conditions (Fig. 1 A). Expression of MMP9, another critical protease in ECM remodeling activated by STAT3, was unchanged in STAT3-CKO astrocytes. Expression of MMP2 was also significantly less in STAT3-CKO astrocytes versus WT astrocytes after challenge with lysophosphatidic acid (LPA), or in vitro injury (wound scratch; Fig. 1 B), consistent with the role of STAT3 in astrocytes after injury. To confirm the role of STAT3 in regulating MMP2, we used gelatin zymography to assess levels of MMP2 in medium collected from WT astrocytes versus STAT3-CKO astrocytes in culture. This assay confirmed the significantly reduced secretion of MMP2 in STAT3-CKO astrocytes, compared with WT astrocytes (Fig. 1 C). To test whether reduced secretion of MMP2 impairs astrocyte migration, we examined the ability of STAT3-CKO astrocytes to migrate through Matrigel (BD). As a positive control, we also tested astrocytes from *Mmp2*$^{-/-}$ mice. STAT3-CKO astrocytes exhibited defective invasion through Matrigel, and reduced invasion of MMP2-KO astrocytes indicated that MMP2 is necessary for invasion through Matrigel (Fig. 1 D). MMP2-KO astrocytes did not show any significant reduction in migration in a trans-well assay compared with WT astrocytes, indicating that MMP2 does not affect nonproteolytic migration in this assay (Fig. 1 E). Although the reduction of MMP2 secretion by STAT3-CKO astrocytes is a relevant observation in the context of SCI, where MMP2 promotes scar formation (Hsu et al., 2006), the noninvolvement of MMP2 in trans-well migration indicates that other effectors of STAT3 are involved in the proteolysis-independent movements of astrocytes.

STAT3 is a pace keeper of adhesion dynamics in migrating astrocytes

STAT3 is known to stabilize the microtubules in various cells (Ng et al., 2006; Verma et al., 2009). Ablation of STAT3 in astrocytes did not result in the expected destabilization of microtubules (Fig. 2 A). Quantitative analysis showed that α-tubulin immunoreactivity (IR) was even moderately increased in STAT3-CKO astrocytes, for an unknown reason. The formation of glial scars involves the reorientation of astrocytic processes, a process which is defective in STAT3-ablated reactive astrocytes (Wanner et al., 2013). We therefore evaluated the response of astrocytes to an in vitro wound-scratch, an established model in studies of polarization (Etienne-Manneville, 2006). Surprisingly, centrosomes (means ± SEM; 65.1% ± 7.1 and 61.7% ± 5.1 for WT and STAT3-CKO, respectively) and Golgi apparatus (64.8 ± 6.2% and 60.2 ± 1.8%, respectively) showed normal polarization in STAT3-CKO astrocytes (Fig. 2 B), suggesting that the defective scarring by STAT3-ablated astrocytes is not a result of defective polarization. However, the protrusions formed in response to wounding were significantly shorter in STAT3-CKO astrocytes than they were in the WT counterparts (Fig. 2 C). In addition, the focal adhesions (FAs) of STAT3-CKO astrocytes were significantly longer than those of WT cells (Fig. 2 D). To evaluate FA functionality, we examined the migration of STAT3-CKO astrocytes on inhibition of FAK. Inhibition of FAK reduced the migration of WT astrocytes in a dose-dependent manner (ultimately down to the level of the reduced migration observed in STAT3-CKO), but the migration of STAT3-CKO cells was not significantly affected by PF573228, which suggests that FAK-dependent migration is constitutively

defective in STAT3-CKO astrocytes (Fig. 2 E). However, the activation level of FAK, as assessed by the phosphorylation levels of tyrosines 397 and 576, was not reduced in STAT3-CKO astrocytes (Fig. 2 F), indicating that the defect in FAK-dependent migration is not due to a defect in FAK enzymatic activity. This led us to evaluate whether the effect of STAT3 on migration depends on the strength of cell-substratum adhesion (net adhesion). At any applied concentration of laminin, migration of STAT3-CKO astrocytes was significantly less than that it was for WT astrocytes (Fig. 2 G), which excludes the involvement of cell-adhesion strength, the effect of which on migration varies with the concentration of substrate ECM (DiMilla et al., 1991).

We then examined FA dynamics using time-lapse imaging of RFP-CrkI (Nagashima et al., 2002) in migrating astrocytes (Fig. 2 H and Video 1). Coordination between forward motion of the cells and FA dynamics appeared disrupted in STAT3-CKO astrocytes. In STAT3-CKO cells, FAs that formed at the tips of lamellipodia persisted beyond the lamella, whereas the FA in WT cells disassembled once they were located within a zone ∼20–25 µm from the leading edge. Quantitative analysis confirmed that the lifetime of the FA was significantly longer in migrating STAT3-CKO astrocytes (Fig. 2 I).

Loss of STAT3 results in defective disassembly of FAs

To investigate the possibility that FA disassembly is defective in STAT3-CKO astrocytes, we controlled the induction of FAs by treating serum-starved astrocytes with LPA (Ridley and Hall, 1992). LPA-induced FAs were longer in STAT3-CKO astrocytes than they were in WT astrocytes (Fig. 3, A and B). Colocalization of phospho-Y418-Src with paxillin and F-actin indicated that activated Src family kinases were concentrated in mature FAs in astrocytes (Fig. 3 C), which is consistent with their role in FA disassembly (Lee et al., 2010). These astrocytes were subsequently treated for an additional 45 min with an inhibitor of Src kinases, SU6656, to inhibit FA disassembly (Lee et al., 2010). As expected, Src inhibition resulted in significant elongation of FAs in WT astrocytes. In STAT3-CKO astrocytes, inhibition of Src did not result in FA elongation (Fig. 3, A and B), indicating that Src-dependent disassembly of FA is deficient in these cells. In a trans-well assay, inhibition of Src kinases consistently reduced the migration of WT astrocytes in a dose-dependent fashion but did not affect STAT3-CKO astrocytes (Fig. 3 D). Phospho-Src levels by immunoblotting showed that Src signaling is not reduced in STAT3-CKO astrocytes, compared with that in WT astrocytes (Fig. 3 E).

Regulation of RhoA by STAT3 determines actomyosin tonus and migration in astrocytes.

Actomyosin-generated tensions regulate FA dynamics (Ridley and Hall, 1992; Wolfenson et al., 2011), so we examined F-actin and actomyosin contractility in STAT3-CKO astrocytes. Astrocytes exhibit a high degree of morphological diversity under usual culture conditions, which makes analysis of stress fibers difficult. However, we found that astrocytes undergo stereotypical changes during the spreading that follows replating. In this context, the central stress fibers that formed during the spreading of STAT3-CKO astrocytes on laminin were much stronger than those observed in WT astrocytes (Fig. 4 A). Unlike the resistant, peripheral actin ring, these central stress fibers were sensitive to inhibition of RhoA effector kinase (ROCK) by H1152 (Fig. 4 B). Evaluation of actomyosin contractility in a collagen-gel assay showed that WT and STAT3-CKO astrocytes contract to the same extent on stimulation by TGF-α (Fig. 4 C). In both cell types, inhibition of ROCK by H1152 prevented such contraction, and even induced relaxation, which confirmed the specificity of the test. In the absence of contractile stimulation, STAT3-CKO astrocytes exhibited more basal actomyosin tonus than WT astrocytes did.

Given the role of the small GTPase RhoA in actin dynamics (Ridley and Hall, 1992), we next examined the activation of RhoA in STAT3-CKO astrocytes. We found that although RhoA expression level was significantly reduced in STAT3-CKO astrocytes (Fig. 4 E), the activation of RhoA was significantly increased in STAT3-CKO astrocytes under usual culture conditions (Fig. 4 D). Evaluation of downstream signaling indicated that this constitutive activation of RhoA is potent in STAT3-CKO astrocytes. The phosphorylation of myosin light chain-2 (MLC2) was increased during the usual culture conditions (Fig. 4 F). In addition, the phosphorylation of MLC2 on stimulation by leukemia inhibitory factor (LIF) was stronger and was delayed in STAT3-CKO astrocytes (Fig. 4 G), compared with WT astrocytes. Suppressor of cytokine signaling-3 (SOCS3), a negative regulator of LIF receptor signaling (Takahashi et al., 2003), was not induced in response to LIF in STAT3-CKO astrocytes, in contrast to the transient induction observed in WT ones (Fig. 4 G), which suggests that it may enhance the deregulation of the RhoA–ROCK pathway in STAT3-CKO astrocytes.

We next examined the role of RhoA deregulation in the defective migration of STAT3-CKO astrocytes. Although the inhibition of RhoA-GTPase by a cell-permeable C3 exoenzyme significantly reduced the trans-well migration of WT astrocytes, STAT3-CKO astrocytes appeared insensitive to that inhibition (Fig. 4 H). Inhibition of ROCK by either of two drugs, Y27632 or H1152, produced similar results; unlike WT cells, the migration of STAT3-CKO astrocytes was insensitive to ROCK inhibition (Fig. 4, I and J). Immunoblotting showed that strong inhibition of ROCK in astrocytes, as confirmed by the markedly reduced phosphorylation of MLC2, did not affect the phosphorylation level of Y705 in STAT3 (Fig. 4 K). This excludes the possibility that the reduction of WT astrocyte migration is due to the inhibition of STAT3 itself by ROCK inhibitors, as suggested in a previous study (Sanz-Moreno et al., 2011). Downstream targeting of the Rho/ROCK axis through inhibition of MLC kinase with ML-7 or myosin II ATPase with blebbistatin also indicated that the decreased migration of STAT3-CKO astrocytes is caused by deregulation of the RhoA–ROCK pathway (Fig. 4, L and M). These in vitro data suggest that constitutive activation of RhoA in STAT3-CKO astrocytes impairs actomyosin tonus, FA dynamics, and migration.

Next, we sought to identify the mechanisms by which RhoA is constitutively activated in STAT3-CKO astrocytes. Using quantitative real-time PCR, we first examined the expression levels of obvious candidates, i.e., guanine nucleotide exchange factors (GEFs) and GTPase-activating proteins (GAPs), that might contribute directly to the activation of RhoA in astrocytes. None of the GEFs examined were up-regulated (Fig. S1 A), and none of the GAPs examined were down-regulated (Fig. S1 B), in STAT3-CKO astrocytes.

We next examined ezrin, radixin, and moesin (ERM) proteins, which are involved in multiple aspects of cell migration (Clucas and Valderrama, 2014) and antagonize the activity of RhoA (Speck et al., 2003). Expression levels of these three pro-

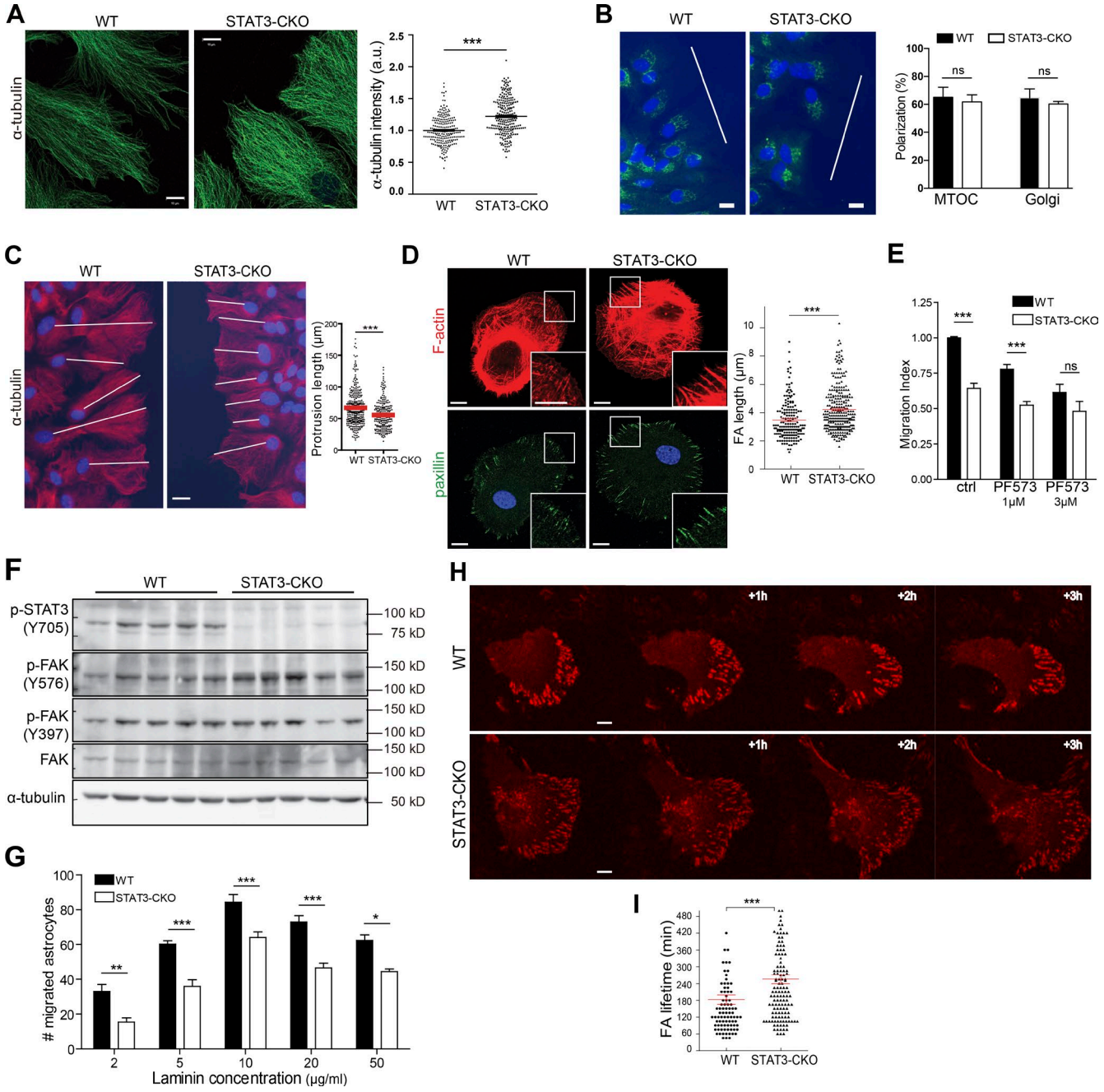

Figure 2. **STAT3 is a pace keeper of adhesion dynamics in migrating astrocytes.** (A) Ablation of STAT3 in astrocytes does not result in the destabilization of the microtubule cytoskeleton. Quantitative analysis even shows a moderate increase of α-tubulin IR in STAT3-CKO astrocytes (unpaired *t* test, *n* = 221 and 241 WT and STAT3-CKO astrocytes, respectively). Bars, 10 µm. (B) The polarization of STAT3-CKO astrocytes in response to a wound scratch is not significantly affected. Green, β-COP; blue, nuclear staining by Hoechst. Bars, 20 µm. MTOC, microtubule organizing center. (C) The protrusions formed 16 h after wounding are shorter in STAT3-CKO astrocytes (*n* = 324 WT and 225 STAT3-CKO cells, three independent experiments, Mann-Whitney *U* test). Bar, 20 µm. (D) STAT3-CKO astrocytes seeded onto laminin exhibit longer FAs than WT cells. Bars, 10 µm. We analyzed 175 and 279 FAs, respectively, from seven WT and eight STAT3-CKO astrocytes. (Mann-Whitney *U* test). (E) The effect of FAK inhibitor (PF573228; 0, 1, and 3 µM from left to right) on the migration of WT and STAT3-CKO astrocytes. (F) Phosphorylation levels of FAK on Y576 and Y397 exclude defective activation of FAK in STAT3-CKO cells. (G) Control of astrocyte migration by STAT3 does not involve modulation of adhesion strength. (H) Time-lapse analysis of migrating astrocytes transfected with RFP-Crkl revealed that STAT3 is necessary for the timely coordination of FA dynamics with forward cell locomotion (Video 1). Bars, 10 µm. (I) Quantitative analysis confirmed an extended FA lifetime in STAT3-CKO cells (*n* = 89 and 130 FAs analyzed in 13 WT and 13 STAT3-CKO astrocytes, respectively; Mann-Whitney *U* test). ns, not significant. Error bars indicate ±SEM. *, P < 0.05; **, P < 0.01; ***, P < 0.001.

teins were not significantly modified in STAT3-CKO astrocytes compared with WT astrocytes. In contrast, immunoblotting with an antibody recognizing threonine-phosphorylated residues (Thr567 of ezrin, Thr564 of radixin, and Thr558 of moesin), which are known to have key roles in regulating ERM protein conformation and function, revealed a significant reduction in the phosphorylation of ezrin in STAT3-CKO astrocytes under usual culture conditions, i.e., without any specific experimental stimulus (Fig. 4 N). This suggests that the constitutive activation of RhoA in STAT3-CKO astrocytes is attributable to reduced

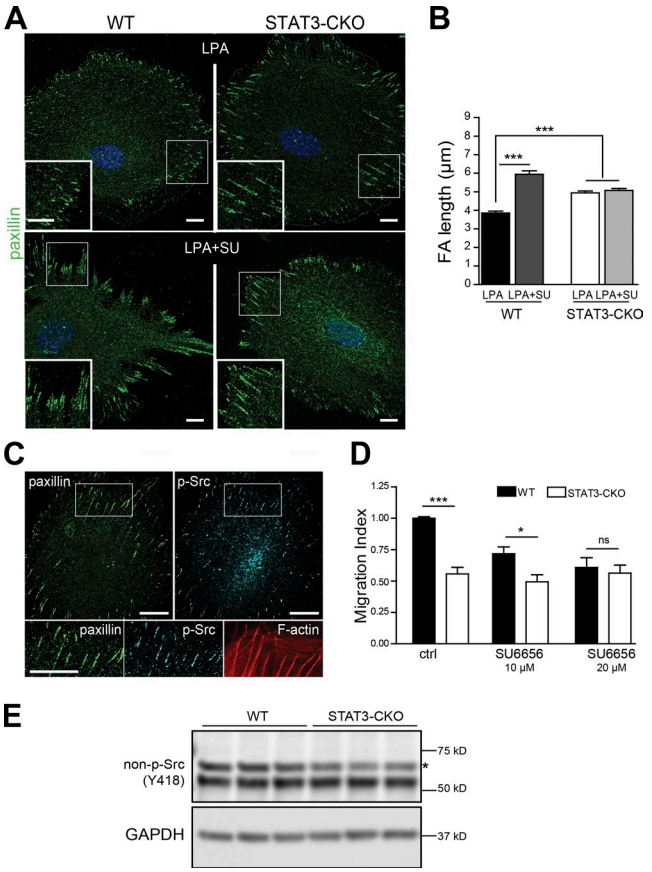

Figure 3. **Loss of STAT3 results in defective focal adhesion disassembly.** (A and B) Longer LPA-induced FAs and their defective elongation on Src inhibition suggest that FA disassembly is defective in STAT3-CKO astrocytes (n = 239 and 169 FAs in WT, respectively, n = 273 and 202 FAs in STAT3-CKO, respectively; Kruskal-Wallis test, followed by Dunn's test). Bars, 10 µm. (C) Colocalization of p-Src with paxillin and F-actin indicates that p-Src is concentrated in mature FA. Bars, 10 µm. (D) In contrast to WT astrocytes, the inhibition of Src kinases has no effect on the trans-well migration of STAT3-CKO astrocytes (ANOVA, two ways; and Bonferroni's test). (E) Western blotting of astrocyte lysates with a specific antibody that detects Src (and other Src family members) only when dephosphorylated at tyrosine 416 indicates that the activation of Src family kinases is not reduced in STAT3-CKO astrocytes. The asterisk indicates the position of the band of Src kinases (~60 kD), whereas the lower band is likely not specific. Ctrl, control. ns, not significant. Error bars indicate ±SEM. *, $P < 0.05$; ***, $P < 0.001$.

phosphorylation of ezrin. GRK2, a kinase that phosphorylates ezrin (Cant and Pitcher, 2005), has been shown to positively regulate cell migration (Penela et al., 2009); we thus examined its expression level in astrocytes. Expression of GRK2 is not significantly changed in STAT3-CKO astrocytes versus WT astrocytes (Fig. 4 O). The reason for the reduced phosphorylation of ezrin in STAT3-CKO astrocytes is unknown.

Corralling of astrocytes by leukocytes relies on the Rho/ROCK pathway

Ablation of STAT3 in reactive astrocytes results in the defective seclusion of leukocytes and meningeal fibroblasts that infiltrate spinal cord lesions (Okada et al., 2006; Herrmann et al., 2008). As RhoA mediates the signaling of various repulsive pathways (Fujita and Yamashita, 2014), we wondered whether RhoA is necessary for the corralling of inflammatory cells by reactive astrocytes (Wanner et al., 2013). We observed that in vitro corralling of microglia and bone marrow–derived macrophages by astrocytes was lost on inhibition of the RhoA/ROCK pathway (Fig. 5 and Fig. S2), which suggests that deregulation of the RhoA/ROCK pathway in STAT3-CKO astrocytes affects not only the dynamics of reactive astrocytes themselves but also their ability to repel infiltrating cells within CNS lesions.

We next searched for in vivo evidence to support these in vitro findings.

Nestin-Cre mouse allows specific genetic targeting of lesion-proximal, reactive astrocytes

We first speculated that a subset of elongated, reactive astrocytes located in the immediate vicinity of CNS traumatic lesions, which are known to express the intermediate filament protein Nestin in the acute phase after focal brain injury (Suzuki et al., 2012), might be more likely to contribute directly to glial scar formation than the wider population of GFAP-positive, reactive astrocytes. Examination of Nestin IR in a contusive SCI model confirmed that up-regulation of Nestin selectively identifies lesion-proximal, reactive astrocytes in the injured spinal cord (Fig. S3). To target this subpopulation of reactive astrocytes, we compared three lines of *Nestin*-EGFP reporter mice: *Nestin*-EGFP(A) (Kawaguchi et al., 2001), *Nestin*-EGFP(B) (Yamaguchi et al., 2000), and *Nestin*-CCE (Okada et al., 2006; Fig. 6). The conditional mouse line *Nestin*-CCE was particularly interesting. To generate *Nestin*-CCE mice, we crossed *Nestin*-Cre mice (Betz et al., 1996) with another transgenic line (Kawamoto et al., 2000) carrying a CAG promoter-loxP-CAT-loxP-EGFP (CAG-CAT$^{loxP/loxP}$-EGFP) reporter gene construct, which directs expression of EGFP on Cre-mediated recombination. Remarkably, in *Nestin*-CCE, there was no detectable fluorescence in the spinal cord of sham-operated animals, even in the area surrounding the central canal in which stem/progenitor cells are typically found (Fig. 6 A), in contrast with the two other Nestin mouse lines examined. Moreover, GFAP$^+$ and Nestin$^+$, which were reactive to astrocytes surrounding the lesion, were readily identified by strong EGFP fluorescence in injured *Nestin*-CCE animals (Fig. 6 B), suggesting that specific genetic targeting of lesion-proximal, reactive astrocytes occurred in *Nestin*-CCE mice.

Modifications of RhoA pathway components in the injured spinal cords of *Nestin-Stat3*$^{-/-}$ mice.

We used this *Nestin*-Cre driver line to examine the effect of STAT3 deletion on the morphology of lesion-proximal, reactive astrocytes in the spinal cord. Using GFAP-Cre driver mice undergoing severe crush SCI, Sofroniew and colleagues have shown that STAT3-ablated, reactive astrocytes fail to hypertrophy (Herrmann et al., 2008) and that astrocytic processes fail to assemble in bundles (Wanner et al., 2013). In relation to the reduced length of α-tubulin protrusions that we observed after wound scratch in vitro (Fig. 2 C), we performed a wound stab in the dorsal spinal cord of adult *Nestin-Stat3*$^{-/-}$ and WT mice to examine the appearance of reactive astrocytes located proximal to the lesion. Simultaneous immunostaining for both GFAP and AQP4 allowed clear visualization of the astrocyte processes in the injured area located in the dorsal white matter (Fig. 7). At 7 d postinjury (dpi), reactive astrocytes at the lesion site were clearly elongated with a few, thick processes extending toward the lesion site in WT mice (Fig. 7). In con-

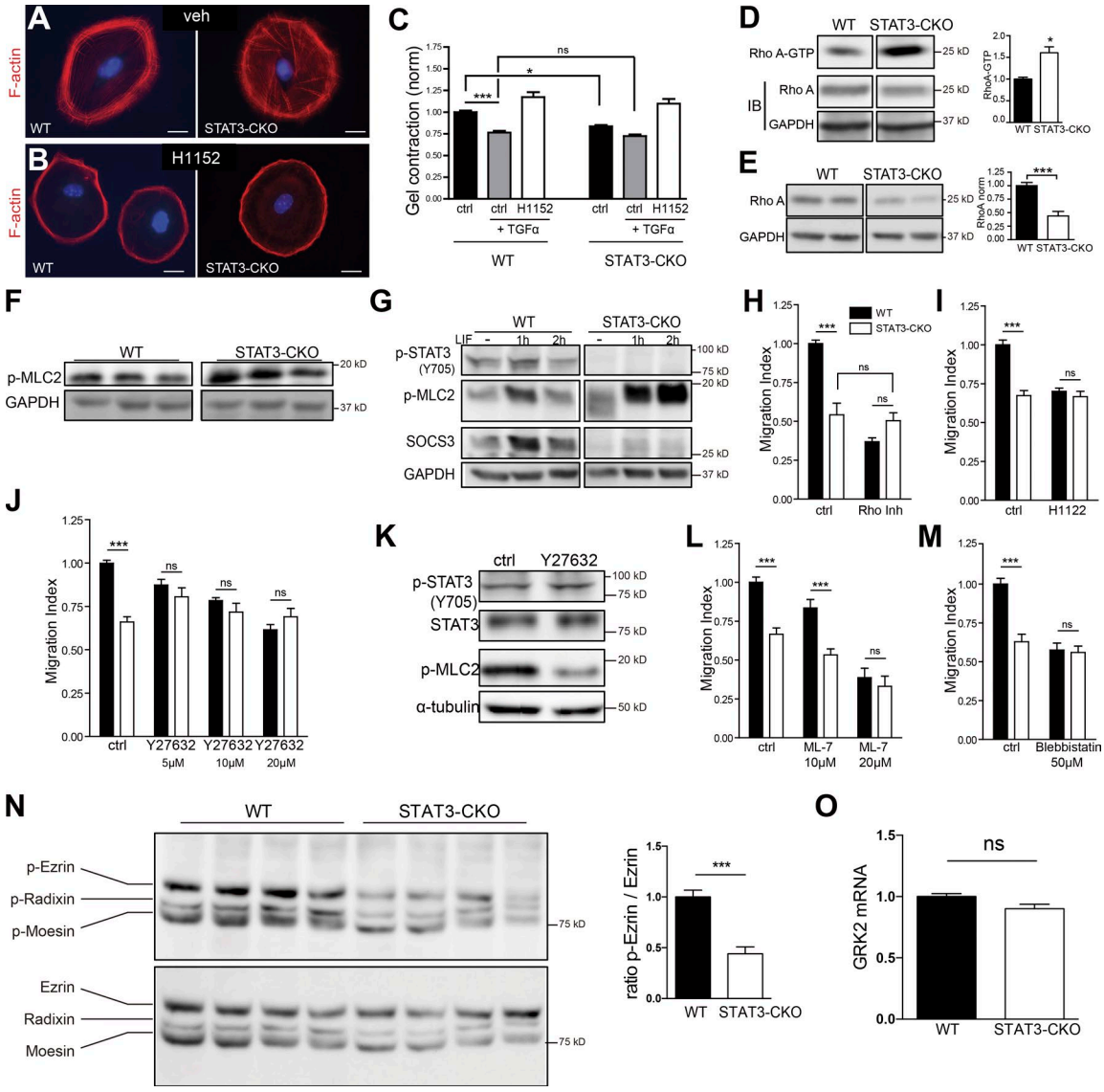

Figure 4. **Regulation of RhoA by STAT3 determines actomyosin tonus and migration in astrocytes.** (A) Central stress fibers that formed 15 h after seeding onto laminin are stronger in STAT3-CKO astrocytes than in WT astrocytes. Bars, 20 µm. (B) These ventral stress fibers are sensitive to inhibition of ROCK in contrast to the peripheral actin ring, which is resistant. Bars, 20 µm. (C) Collagen gel contraction assay revealed an elevated actomyosin tonus in STAT3-CKO astrocytes, whereas contraction in response to TGF-α is not modified when compared with WT cells (data shown from three independent experiments in triplicate, one-way ANOVA followed by Bonferroni's test). (D) RhoA is constitutively activated in STAT3-CKO astrocytes ($n = 4$ per group; Mann-Whitney *U* test; P = 0.0286). (E) Significant down-regulation of RhoA in STAT3-CKO astrocytes (Mann-Whitney *U* test, $n = 7$ and 9, in WT and STAT3-CKO, respectively; P = 0.0007). (F) Phosphorylation of MLC2 is increased in STAT3-CKO astrocytes in the usual culture conditions and after stimulation with human LIF (hLIF; G). The kinetics and amplitude of myosin light chain (MLC) phosphorylation are changed in STAT3-CKO astrocytes. Note the absence of induction of SOCS3 in response to hLIF in STAT3-CKO cells and that bands in (G) were from two separate gels that were processed in parallel. (H) In contrast to WT astrocytes, migration of STAT3-CKO astrocytes in the trans-well assay is insensitive to inhibition of RhoA-GTPase with 2 µg/ml of cell-permeable C3 exoenzyme (CT04). (I and J) Migration in the presence of two different ROCK inhibitors resulted in the same observation as in (H). (K) The activation level of STAT3 in astrocytes is not reduced upon ROCK inhibition. WT astrocytes were treated for 6 h with 20 µM Y27632. Treatment with MLC kinase inhibitor (L) or myosin II ATPase inhibitor (M) further showed that STAT3 is necessary for the RhoA-GTPase–dependent migration of astrocytes. (N) Phosphorylation of ezrin on Thr567 is selectively reduced in STAT3-CKO astrocytes, compared with WT astrocytes under the usual culture conditions (Mann-Whitney *U* test, P < 0.0001, $n = 6$ per group). (O) The level of GRK2 mRNA is unchanged in STAT3-CKO astrocytes versus WT astrocytes. (Normalization is made with GAPDH, Mann-Whitney *U* test, $n = 5$ per group). Ctrl, control; ns, not significant; Veh, vehicle. Error bars indicate ±SEM. *, P < 0.05; ***, P < 0.001.

trast, STAT3-ablated, reactive astrocytes appeared very different, with no obvious elongation and, therefore, no preferential orientation toward the lesion (Fig. 7). This in vivo observation is consistent with the morphological changes observed in vitro and with a possible modification of RhoA in the injured spinal cord of *Nestin-Stat3*$^{-/-}$ mice.

This led us to examine the expression and activation of RhoA in vivo. We observed that RhoA was significantly down-regulated in the spinal cords of *Nestin-Stat3*$^{-/-}$ mice at 5 d after contusive injury (Fig. 8 A), in agreement with our observation in primary astrocytes (Fig. 4 E). Furthermore, the quantification of the pool of active RhoA (RhoA-GTP) by G-Lisa assay showed an augmentation of activated RhoA in the injured spinal cords of *Nestin-Stat3*$^{-/-}$ mice at 5 dpi but which did not reach statistical significance (Fig. 8 B). Immunostaining for phosphorylated-ERM proteins in injured spinal cords showed indis-

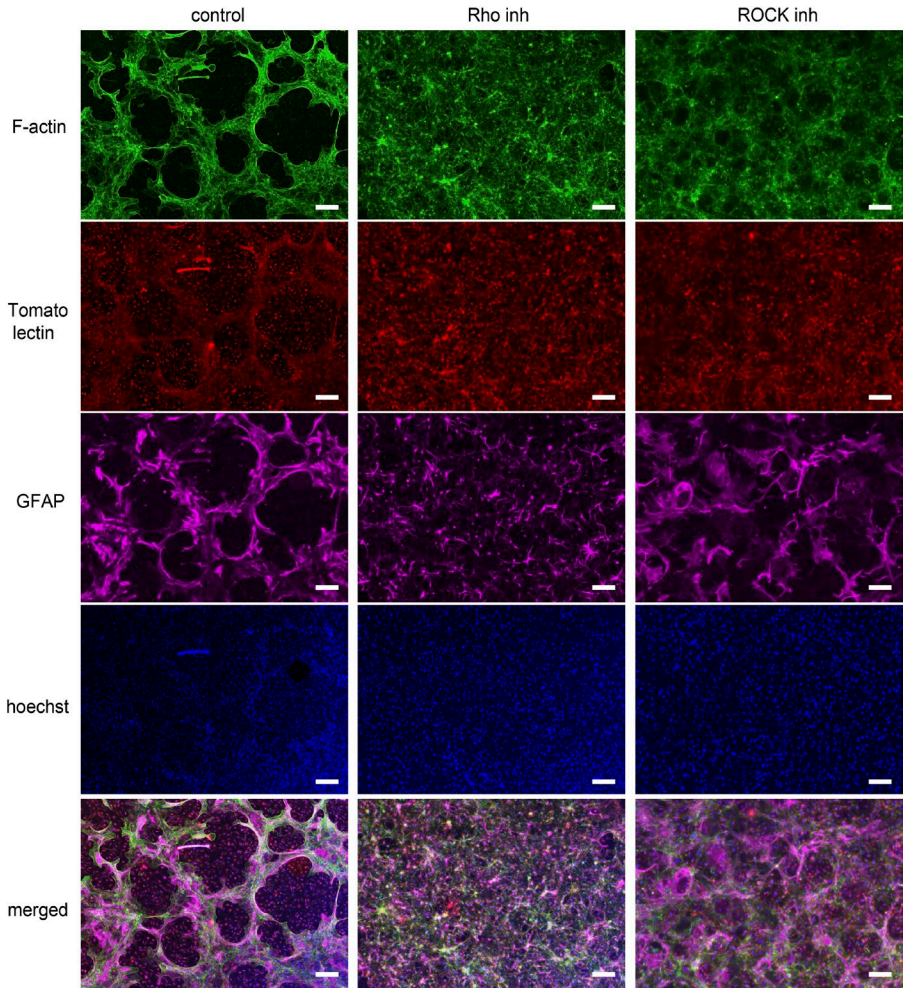

Figure 5. **Corralling of microglial cells by astrocytes relies on the Rho–ROCK pathway.** In co-cultures, the corralling of microglial cells into segregated clusters by WT astrocytes is prevented by Rho and ROCK inhibitors. Bars, 200 µm.

tinct expression of p-ERM IR in both reactive astrocytes and nonastrocyte cells (i.e., based on their morphology, very likely leukocytes) within the lesion in WT mice (Fig. 8 C). In contrast, p-ERM IR appeared specifically reduced in the reactive astrocytes of *Nestin-Stat3*$^{-/-}$ mice (Fig. 8 C). Z-stack analysis at high magnification by confocal microscopy confirmed that p-ERM IR was localized within both nonastrocytes cells and reactive astrocytes bordering the lesion in WT mice (Fig. 8 D and Video 2). In contrast, p-ERM IR was specifically reduced in the reactive astrocytes of *Nestin-Stat3*$^{-/-}$ mice, whereas the signal was not affected in surrounding nonastrocyte cells (Fig. 8 D and Video 3). These observations suggest that the regulation of RhoA by STAT3 observed in primary astrocytes also occurs within reactive astrocytes in the context of SCI.

miR-21–mediated repression of PTEN by STAT3 controls adhesion dynamics and astrocyte migration

Phosphatase and tensin homologue (PTEN) controls astrocyte migration and inhibits the activation of Rac1 (Dey et al., 2008), an antagonist of RhoA. In various cell types, STAT3 represses PTEN through the expression of miR-21 (Iliopoulos et al., 2010), so we investigated whether PTEN is involved in the regulation of astrocytes dynamics by STAT3. Real-time quantitative PCR showed a significant reduction of miR-21 in STAT3-CKO astrocytes in comparison to WT astrocytes (Fig. 9 A). Consistent with derepression from the down-regulation of miR-21, PTEN levels were significantly increased in STAT3-CKO astrocytes compared with those of WT mice (Fig. 9 B). We then examined the activation of the protein kinase Akt, an indirect marker of PTEN phosphatase activity. The phosphorylation of Akt on Ser473 was consistently and significantly reduced in STAT3-CKO astrocytes. Immunocytochemistry indicated that PTEN is unambiguously distributed in the cytoplasm and nuclei of STAT3-CKO astrocytes in vitro (Fig. 9 C). Next, we examined regulation of PTEN by STAT3 in vivo. miR-21 is transiently up-regulated after SCI (Strickland et al., 2011), so we examined its expression in the injured spinal cords of WT and *Nestin-Stat3*$^{-/-}$ mice at 5 dpi; however, we observed only a nonsignificant reduction of miR-21 in the contused spinal cords of *Nestin-Stat3*$^{-/-}$ mice (Fig. 9 D). Although PTEN IR is very weak and sparse in the sham spinal cord, contusive SCI induced strong up-regulation of PTEN IR (Fig. 9 E). Confocal microscopy showed elevated neuronal expression of PTEN in both WT and *Nestin-Stat3*$^{-/-}$ mice at 5 dpi (Fig. 9 F). In contrast, the up-regulation of PTEN in reactive astrocytes appeared stronger in *Nestin-Stat3*$^{-/-}$ mice than it did in WT mice (Fig. 9 F). These data indicate that STAT3 represses PTEN expression, likely via miR-21, in reactive astrocytes in vitro and in vivo after SCI.

To examine whether PTEN repression is involved in the control of astrocyte migration by STAT3, we generated mice harboring conditional, heterozygous deletions of both STAT3 and PTEN in reactive astrocytes (*Nestin-Stat3*$^{+/-}$*/Pten*$^{+/-}$). Reduction of PTEN rescued the migration of STAT3$^{+/-}$/

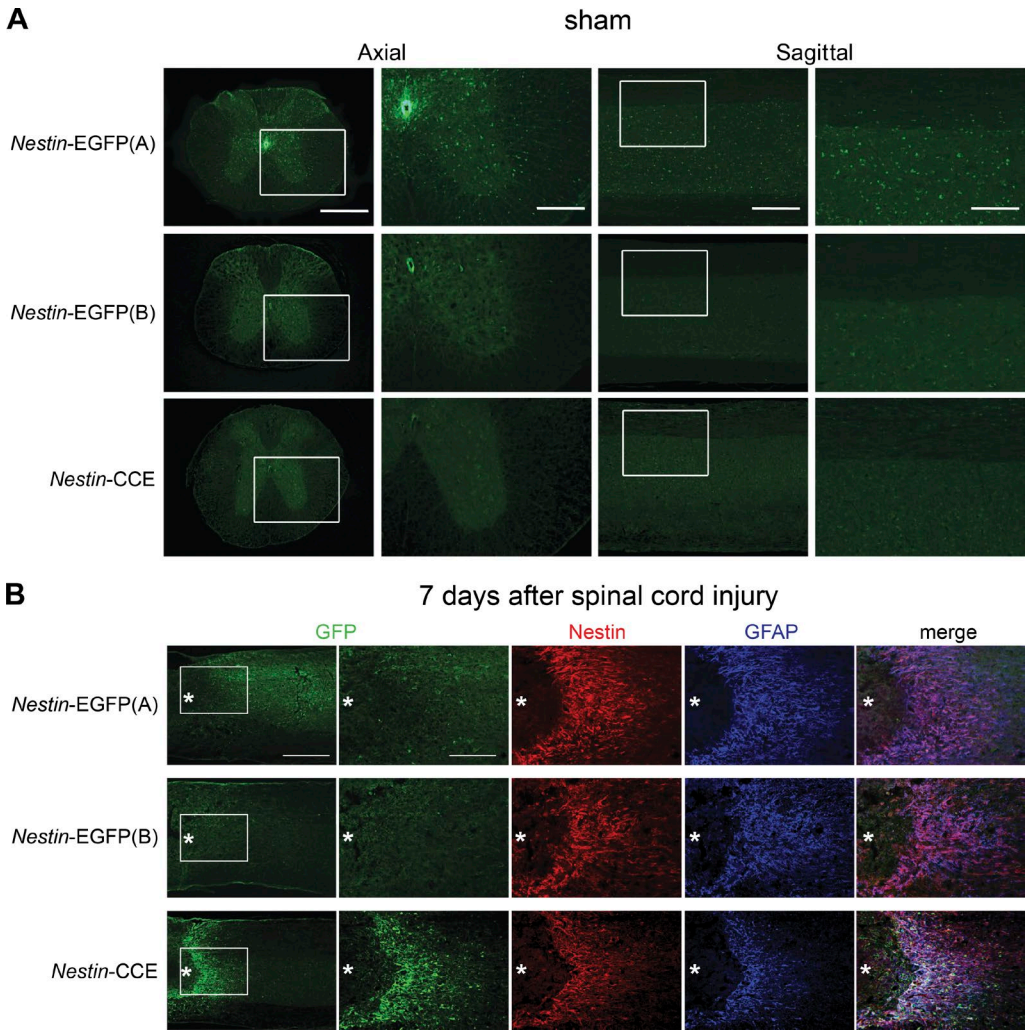

Figure 6. **Specific targeting of reactive astrocytes using *Nestin*-Cre mice.** (A) In contrast with the mouse strains *Nestin*-EGFP(A) and *Nestin*-EGFP(B), the *Nestin*-CCE mouse is characterized by the absence of any notable fluorescence in the spinal cord of sham-operated animals, even surrounding the central canal lodging stem/progenitor cells. Bars: (first and third columns) 500 µm; (second and fourth columns) 200 µm. (B) In contrast, GFAP+- and Nestin+-reactive astrocytes that surround the lesion are easily identified by strong EGFP fluorescence in the spinal cord of *Nestin*-CCE mice (sagittal sections), indicating that *Nestin*-CCE mice undergo specific genetic labeling of reactive astrocytes. Asterisks, lesion center. Bars: (first column) 500 µm; (second column) 200 µm. Refer to Materials and methods for descriptions of the three mouse strain.

PTEN$^{+/-}$ astrocytes in a trans-well migration assay (Fig. 9 G). Inhibition of PI3K by LY294002 resulted in a similar reduction of the migration of WT and STAT3-CKO astrocytes, suggesting that the lipid phosphatase activity of PTEN is not involved in the STAT3-dependent migration of astrocytes (Fig. 9 H). Analysis of LPA-induced FAs showed that PTEN reduction rescued the lengths of FAs in STAT3$^{+/-}$/PTEN$^{+/-}$ astrocytes to levels resembling those in WT astrocytes (Fig. 9, I and J). Moreover, STAT3$^{+/-}$/PTEN$^{+/-}$ astrocytes recovered their sensitivity to SU6656-induced FA elongation (Fig. 9, I and K). These data indicate that the regulation of FA turnover via PTEN is a major mechanism in the control of astrocytes dynamics by STAT3.

Repression of PTEN by STAT3 coordinates glial scar formation

Finally, we examined whether PTEN had an influence on defective glial scar formation in *Nestin-Stat3*$^{+/-}$ mice. In agreement with previous studies (Okada et al., 2006; Herrmann et al., 2008), we observed that the scar borders at 21 dpi are poorly defined in *Nestin-Stat3*$^{+/-}$ mice (Fig. 10, A and B) compared with WT mice. In contrast, *Nestin-Stat3*$^{+/-}$*/Pten*$^{+/-}$ mice harbor scar borders similar to those in WT mice, where the segregation between reactive astrocytes and lesion center is easily defined. Quantitative analysis confirmed that reduction of PTEN in *Nestin-Stat3*$^{+/-}$ background rescues potently glial scar formation (Fig. 10 C). Examples of injury sites in other animals are presented in Fig. S4. Immunostainings for CD11b, a marker of inflammatory cells, and for fibronectin, a fibroblast marker, supported these observations because the interface between the lesion center and the reactive astrocytes was readily delineated in WT and *Nestin-Stat3*$^{+/-}$*/Pten*$^{+/-}$ mice, compared with the diffuse border in *Nestin-Stat3*$^{+/-}$ mice (Fig. 10 D).

Discussion

Recent studies have dramatically revised our understanding of the role of reactive astrocytes. Lesion scarring by reactive

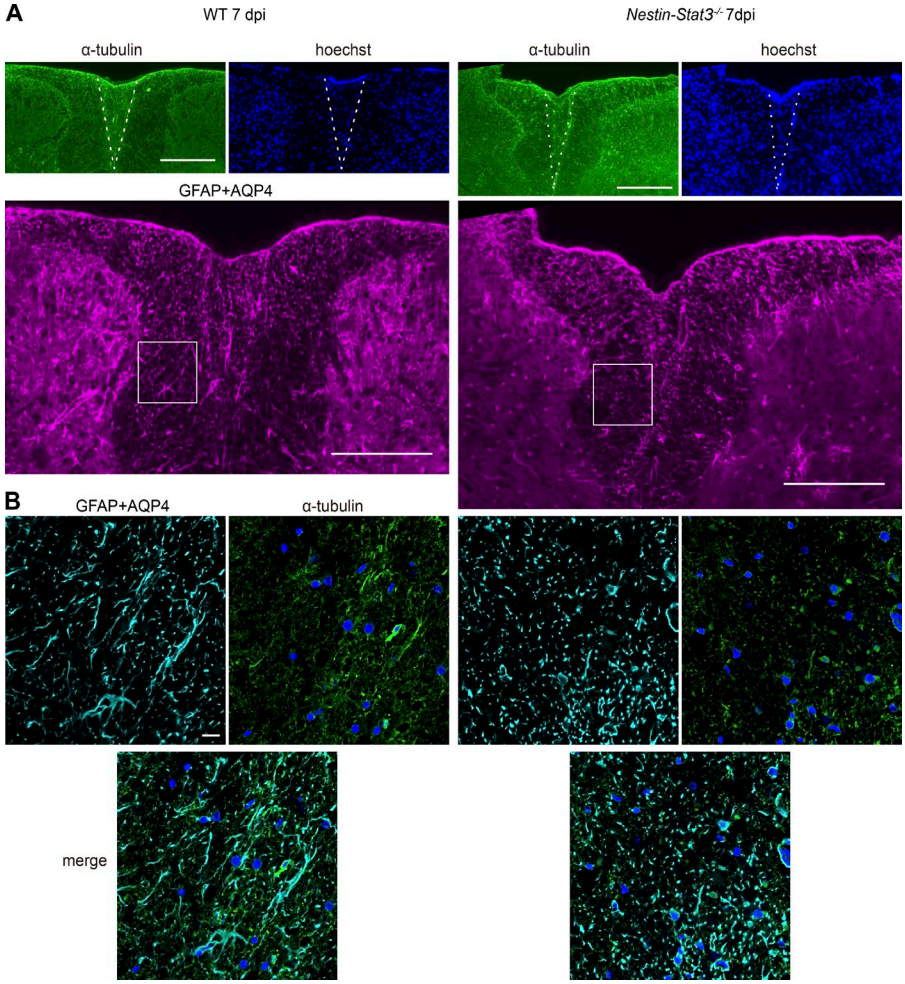

Figure 7. **Altered morphology of reactive astrocytes in *Nestin-Stat3*$^{-/-}$ mice 7 d after wound stab.** (A) 7 d after a superficial midline incision was made along the dorsal column of the spinal cord at T10 level, the injured areas can be easily localized on axial sections of spinal cords (dashed lines). Bars, 200 µm. (B) Note the difference of morphology in WT and *Nestin-Stat3*$^{-/-}$ reactive astrocytes adjacent to the injury (confocal analysis). The localization of the fields captured is indicated by the boxes in A. Bar, 20 µm.

astrocytes has been shown to provide benefits in the subacute phase (Bush et al., 1999; Faulkner et al., 2004) and, to some extent, in the chronic phase of CNS injury (Anderson et al., 2016), as well as in models of autoimmune disease (Voskuhl et al., 2009). Although the role of astrocytic STAT3 in glial scar formation has strong support (Okada et al., 2006; Herrmann et al., 2008; Wanner et al., 2013), the precise molecular mechanisms have remained elusive.

Expression of STAT3 is required for normal secretion of MMP2 in astrocytes.

Although MMP2 is known to be a direct transcriptional target of STAT3 (Xie et al., 2004), to our knowledge, it had never been shown that STAT3 actually controls MMP2 expression in astrocytes. Our observation that MMP2 levels are reduced in the conditioned medium of STAT3-CKO astrocytes is relevant, given that MMP-2 promotes functional recovery after injury by regulating the formation of the glial scar and white matter sparing (Hsu et al., 2006). The unaltered trans-well migration of MMP2-KO astrocytes indicates that the regulation of astrocyte dynamics by STAT3 involves another mechanism.

STAT3 regulates FA dynamics and migration

In the present study, for the first time, to our knowledge, we report that STAT3 regulates the morphology and dynamics of FAs. FAs are considered to be important signaling hubs (Kuo et al., 2011), which suggests that regulation of FAs by STAT3, an important factor in several pathological contexts (e.g., inflammation and cancer), may have consequences in important biological processes, such as cell proliferation, differentiation, survival, and the regulation of gene expression. In STAT3-CKO astrocytes, the slower FA dynamics appear to rely on the impaired disassembly of FAs, which become insensitive to inhibition by Src. While Src and FAK are known to be involved in FA disassembly (Jones et al., 2000), they both exhibit normal levels of expression and phosphorylation in STAT3-CKO astrocytes. Even if FA disassembly does occur in cells that express constitutively active RhoA (Ezratty et al., 2005), it has previously been shown that actomyosin-generated tension controls the molecular kinetics of FAs (Wolfenson et al., 2011). This led us to examine stress fibers and actomyosin contractility in astrocytes. We found both to be elevated on ablation of STAT3.

STAT3 tunes RhoA activation through ezrin

We show that STAT3 controls the activation level of RhoA and that this is crucial to astrocyte dynamics and migration. This finding may account for the previous observation that inhibition of STAT3 potently reduces the migration rate only in cancer cells, in which invasion is dependent on actomyosin (Mierke et al., 2011). However, it appears that this scheme cannot be generalized to all cell types because loss of STAT3 expression in mouse embryonic fibroblasts, in contrast, leads to in-

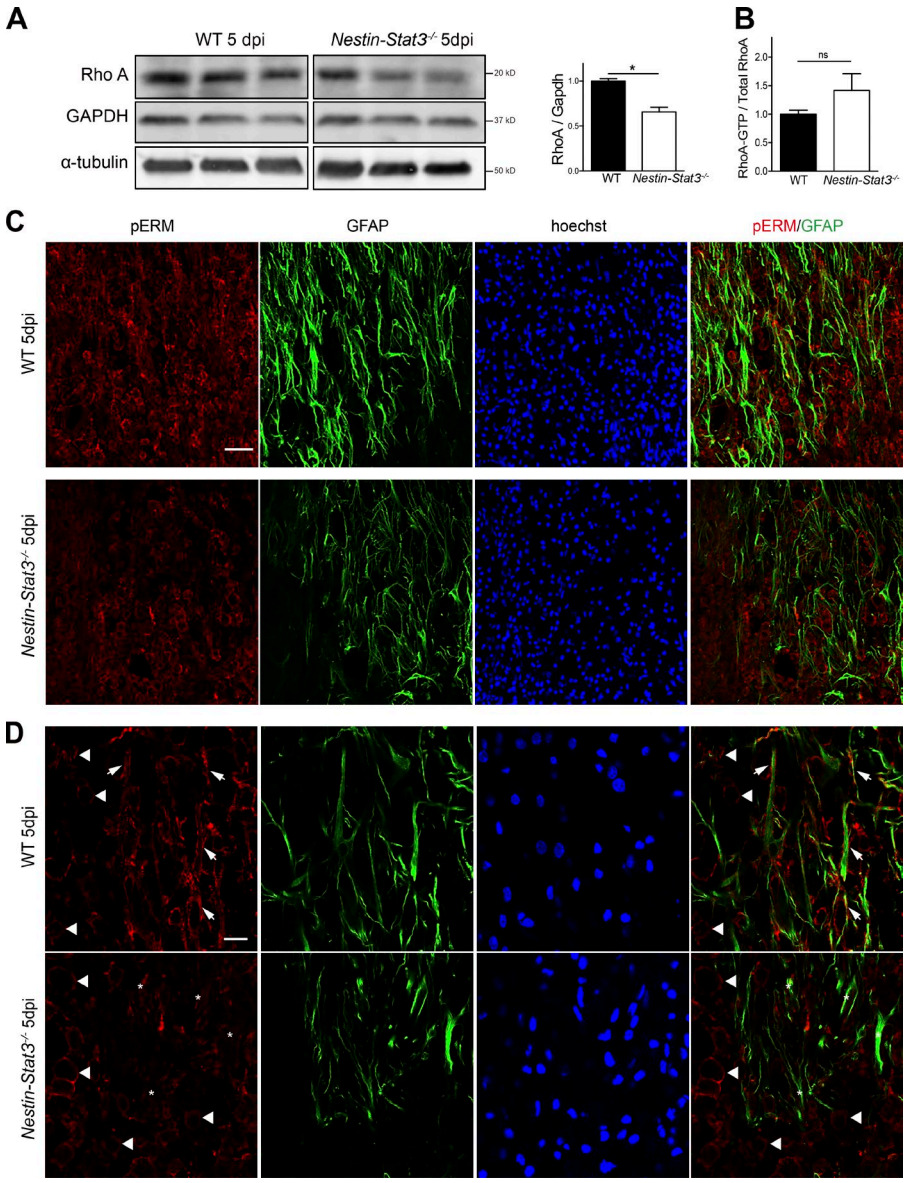

Figure 8. **Modifications of RhoA pathway components in the injured spinal cords of *Nestin-Stat3*$^{-/-}$ mice.** (A) Western blotting shows the expression of RhoA in the spinal cords of *Nestin-Stat3*$^{-/-}$ mice at 5 dpi is reduced compared with WT mice (n = 5 per group, Mann-Whitney U test). (B) The relative amount of activated RhoA (i.e., RhoA-GTP/total RhoA), assessed by G-Lisa assay, exhibits a nonsignificant reduction in the injured spinal cords of *Nestin-Stat3*$^{-/-}$ mice at 5 dpi (n = 6 and 8 mice in WT and *Nestin-Stat3*$^{-/-}$ groups). (C) Phosphorylated ERM proteins are found in both reactive astrocytes and nonastrocyte cells in the lesion border area in the spinal cords of injured WT mice at 5 dpi. In contrast, the p-ERM immunosignal is specifically reduced in reactive astrocytes of injured spinal cords of *Nestin-Stat3*$^{-/-}$ mice (confocal analysis). Bar, 100 µm. (D) High-magnification, confocal analysis allows visualizing the localization of p-ERM in reactive astrocytes (arrows) and nonastrocyte cells (arrowheads) in WT injured spinal cords at 5 dpi. In contrast, in the injured spinal cords of *Nestin-Stat3*$^{-/-}$ mice, whereas the p-ERM signal in nonastrocyte cells is not changed (arrowheads), p-ERM IR is clearly reduced in reactive astrocytes (asterisks). Images shown correspond to a single plane extracted from a 1-µm step Z-stack series. The acquired fields are located at the interface between the lesion center and surrounding reactive astrocytes at 5 dpi. Bar, 20 µm (Videos 2 and 3 display the full Z-stacks). Error bars indicate ±SEM. *, P < 0.05.

creased Rac1 activity (Teng et al., 2009), which antagonizes RhoA (Sander et al., 1999).

Beyond reactive astrocytes dynamics, the regulation of RhoA by STAT3 may take on additional significance in the context of SCI. After SCI, the activation of RhoA in both neuronal and glial cells is indeed rapid and sustained (Dubreuil et al., 2003). The activation of STAT3 observed after injury (Okada et al., 2006) may help to constrain the activation of RhoA. Because the inactivation of Rho–ROCK is required for the generation of Il-1β–induced reactive astrogliosis (John et al., 2004), the constitutive activation of RhoA when STAT3 is ablated is consistent with the observed, attenuated up-regulation of GFAP, failure of astrocyte hypertrophy, and pronounced disruption of astroglial scar formation after SCI in *GFAP*–STAT3-CKO mice (Herrmann et al., 2008). These findings were recently corroborated by the observation that the loss of STAT3 prevents or attenuates most genome-wide changes in astrocytes associated with astrogliosis and scar formation in WT mice (Anderson et al., 2016). Interestingly, John et al. (2004) reported that Il-1β–induced astrogliosis is associated with the disruption of FAs, deactivation of the contractile apparatus of the cell, and activation of ERM adapter proteins. We found that phosphorylation of ezrin is reduced in STAT3-ablated astrocytes, which is consistent with a previous study showing that ezrin regulates proper FA turnover (Hoskin et al., 2015). Our results suggest that ezrin, which is known to inhibit the activation of RhoA (Matsumoto et al., 2014), mediates the inhibition of RhoA by STAT3 in astrocytes.

Our observation that the RhoA–ROCK axis is required for the corralling of leukocytes by reactive astrocytes in vitro is also important because the neuroprotective and myelin-sparing effects of reactive astrocytes during the subacute phase after injury is thought to rely on this walling-off mechanism (Bush et al., 1999; Faulkner et al., 2004; Khakh and Sofroniew, 2015).

Nestin-Cre: a unique strain to target scar-forming, reactive astrocytes

Additionally, we were able to identify lesion-proximal, scar-forming, reactive astrocytes by the expression of Nestin in the acute phase after SCI. We also extended the characterization using *Nestin*-Cre mice, in which recombination does not occur in stem/progenitor cells in the spinal cord. Recombination in

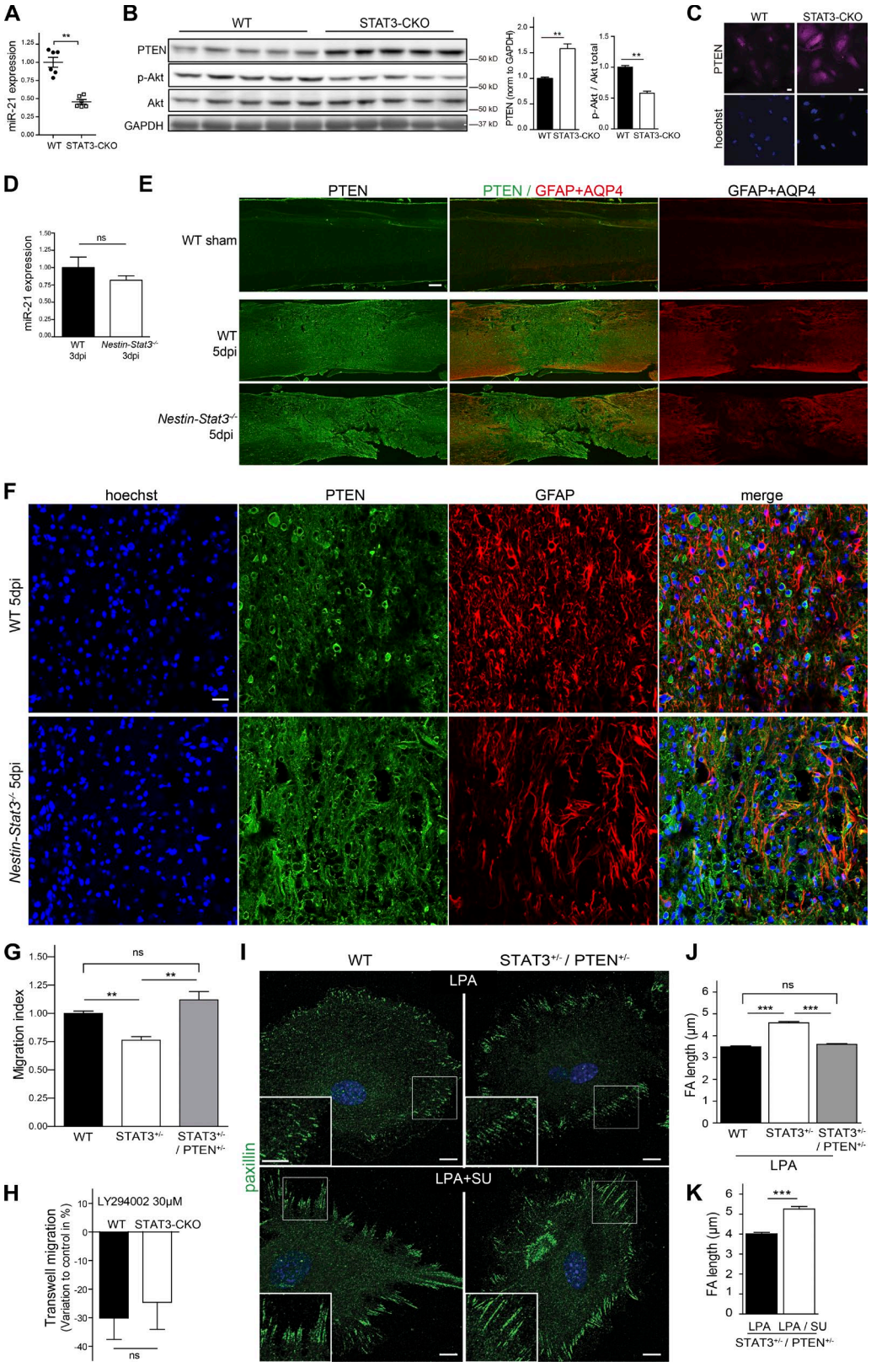

Figure 9. **The miR-21–mediated repression of PTEN by STAT3 controls adhesion dynamics and astrocyte migration.** (A) miR-21 levels are significantly reduced in STAT3-CKO astrocytes (Mann-Whitney *U* test, $n = 6$, P = 0.0022). (B) PTEN is significantly up-regulated in STAT3-CKO astrocytes in vitro, and activation of Akt is accordingly reduced in STAT3-CKO astrocytes ($n = 5$, Mann-Whitney *U* test, P = 0.079 and P = 0.079 for PTEN and p-Akt, respectively). (C) PTEN IR is increased in astrocytes devoid of STAT3 in vitro. Bars, 20 µm. (D) The reduction of miR-21 observed in the spinal cords of *Nestin-Stat3*$^{-/-}$ mice at 3 d after contusive injury is not significant. (E) PTEN is up-regulated in injured spinal cords of both WT and *Nestin-Stat3*$^{-/-}$ mice at 5 dpi compared with sham. (Sagittal sections) Z-stack tile series of images acquired with a KEYENCE BZ-9000 microscope was processed to full focus. Bar, 200 µm. (F) Confocal analysis shows that up-regulation of PTEN in reactive astrocytes after SCI is more pronounced in *Nestin-Stat3*$^{-/-}$ mice. Bar, 50 µm. (G) Reduc-

the adult injured spinal cord of the *Nestin*-Cre mouse does not occur in Hu (ELAVL)-positive neurons and only exceptionally in some GST-π–positive cells (Okada et al., 2006), which may be a subpopulation of astrocytes, as suggested by Herrmann et al. (2008). These findings show that the *Nestin*-CCE mouse enables specific labeling of scar-forming reactive astrocytes in the spinal cord, and thus constitutes a unique tool for their analysis.

Repression of PTEN by STAT3 promotes glial scar formation

In various cell types, STAT3 represses PTEN expression, through miR-21 (Iliopoulos et al., 2010), and PTEN itself regulates astrocyte migration through Rac1 (Dey et al., 2008), an antagonist of RhoA (Sander et al., 1999). While the regulation of PTEN output by RhoA–ROCK has been shown previously (Lima-Fernandes et al., 2011), to our knowledge, regulation of RhoA by PTEN has not been reported. This led us to examine whether PTEN is involved in the STAT3-dependent signaling that regulates astrocytes dynamics. We observed that the reduction of PTEN could rescue FA dynamics and migration of STAT3$^{+/-}$ astrocytes, as well as glial scar formation after SCI. This is consistent with previous studies showing that PTEN prevents glial scar formation. (Goncalves et al., 2015; Chen et al., 2016).

Together with the recent finding that glial scars may, to some extent, promote, rather than exclusively prevent, axon regeneration (Anderson et al., 2016), the deleterious action of astrocytic PTEN in glial scar formation suggests that the therapeutic value of targeting PTEN may extend beyond its direct neuronal action (Liu et al., 2010; Zukor et al., 2013).

Key functions of normal astrocytes, such as glutamate clearance in the synaptic cleft (Pannasch et al., 2014), or their ezrin-dependent contributions to structural, synaptic plasticity (Lavialle et al., 2011), are tightly coupled with changes in their morphology (Heller and Rusakov, 2015), suggesting that the present findings, which relate to the regulation of reactive astrocytes in the context of SCI, may also be relevant to the roles of astrocytes in subnormal CNS.

Materials and methods

Reagents and antibodies

Control solutions (vehicle) used in the study included a 0.1% final concentration of DMSO equal to the amount used to dissolve the test reagents, when necessary. Aphidicolin, blebbistatin, H89, human LIF, LPA, PF573228, and TGF-α were obtained from Sigma-Aldrich. The Rho inhibitor CT04 (Cytoskeleton, Inc.), LY294002 (Promega), H1152 (Tocris Bioscience), Y27632 (Wako Pure Chemical Industries), and ML-7 and SU6656 were obtained from EMD Millipore. The following antibodies were used: mouse β-actin (A1978; Sigma-Aldrich), rat CD11b (MCA711G; Bio-Rad Laboratories), rabbit polyclonal β-COP (PC175; EMD Millipore), mouse fibronectin (610077; BD), rat GFAP (130300; Invitrogen), chicken nestin (NES; supplied by Hiroaki Kanki, AVES Labs, Inc., Tigard, OR), mouse paxillin (610568; BD), rabbit polyclonal pericentrin (PRB-432C; Covance), mouse monoclonal PTEN (559600; BD) for immunoblotting, rabbit monoclonal PTEN (9559; Cell Signaling Technology) for immunofluorescence, mouse monoclonal RhoA (Cytoskeleton, Inc.), rabbit polyclonal SOCS3 (a gift from A. Yoshimura, Keio University School of Medicine, Tokyo, Japan; 18395; IBL-America), mouse monoclonal nonphospho-Y416-Src (2101; Cell Signaling Technology) for blotting and rabbit polyclonal p-Y418-Src (44660G; Invitrogen) for immunostaining, and mouse α-tubulin (T9026; Sigma-Aldrich). Rabbit polyclonal Akt (9271), p-S473-Akt (9277), ERM (3142), p-ERM (3276), FAK (3285), p-Y576-FAK (3281), p-Y397-FAK (3283), GAPDH (2118), myosin light chain-2 (3672), p-S19-MLC (3671), STAT3 (9132), and p-Y705-STAT3 (9131) were all obtained from Cell Signaling Technology. Secondary antibodies used for immunostaining were conjugated to Alexa488, 555, or 647 (Molecular Probes). Peroxidase-conjugated secondary antibodies for Western blotting were obtained from Jackson ImmunoResearch Laboratories, Inc. Texas red–conjugated Tomato lectin was from Vector Laboratories. Cell nuclei were stained using Hoechst 33258 (Thermo Fisher Scientific).

Mice

The MMP2-KO mice (Itoh et al., 1997) were a gift from Shigeyoshi Itohara (Institute of Physical and Chemical Research BioResource Center [RIKEN BRC], Ibaraki, Japan). The PTEN^{LoxP} mice (Suzuki et al., 2001) were a gift from Tak W. Mak (University Health Network, Toronto, Canada) and were provided by the RIKEN BRC through the National BioResource Project of the Ministry of Education, Culture, Sports, Science and Technology (Tokyo, Japan). *Nestin*-EGFP(A) (Kawaguchi et al., 2001), *Nestin*-EGFP(B) (Yamaguchi et al., 2000), *Nestin*-CCE (Okada et al., 2006), and STAT3$^{loxP/loxP}$ mice were previously reported (Okada et al., 2006). In brief, in *Nestin*-Cre mice (Meiji Institute of Health Science, Odawara, Kanagawa, Japan) Cre-recombinase is expressed under the control of the 5.8 Kb *Nes* gene promoter and the 1.8-kb rat second-intronic enhancer (Johansson et al., 2002). To generate *Nestin*-CCE mice, the *Nestin*-Cre mice were crossed with another transgenic line that carried the CAG promoter-loxP-CAT-loxP-EGFP (CAG-CAT$^{loxP/loxP}$-EGFP) reporter gene construct (a gift from J. Miyazaki, Osaka University Graduate School of Medicine, Osaka, Japan; Kawamoto et al., 2000), which directs expression of EGFP upon Cre-mediated recombination.

Cell culture

Primary astrocytes were prepared as previously described (Renault-Mihara et al., 2011) from cortices and striata of 1- or 2-d-old mice. *Nestin*-Cre; STAT3$^{+/-}$/PTEN$^{+/-}$ astrocytes were obtained by mating *Nestin*-Cre^{+}PTEN$^{flox/WT}$ mice with STAT3$^{flox/flox}$ mice. All mice used in this study had the C57BL/6J genetic background.

Isolation of microglial cells was adapted from a previous protocol (Calvo et al., 2005). In brief, cerebral hemispheres from newborn C57BL/6J mice were dissociated by trituration after removal of the meninges. Cells were seeded in DMEM/F12 supplemented with 33 mM glucose, 2 mM L-glutamine, 20 mM $NaHCO_3$, 5 mM Hepes, pH 7.4, 50 IU/ml penicillin, and 5 µg/ml streptomycin and containing 10% heat-inactivated FBS. The culture medium was changed on days 1 and 3. On day 8, fresh medium was supplemented with 20% medium conditioned by L929 cells. Microglial cells were harvested by

tion of PTEN rescued the migration of STAT3$^{+/-}$ astrocytes. (H) WT and STAT3-CKO astrocytes exhibit equivalent reductions of trans-well migration upon inhibition of PI3K. (I and J) The length of LPA-induced FA is rescued to WT values in STAT3$^{+/-}$/PTEN$^{+/-}$ astrocytes (left histogram, n = 810, 793, and 975 FAs of 25 WT; 27 STAT3$^{+/-}$; and 27 STAT3$^{+/-}$/PTEN$^{+/-}$ astrocytes, respectively). (I and K) FAs recover their sensitivity to Src kinase inhibition in STAT3$^{+/-}$/PTEN$^{+/-}$ astrocytes (right histogram, n = 381 and 182 FAs of the LPA alone versus LPA/SU6656 groups, respectively; unpaired t test). Bars, 10 µm. Error bars indicate ±SEM. **, P < 0.01; ***, P < 0.001.

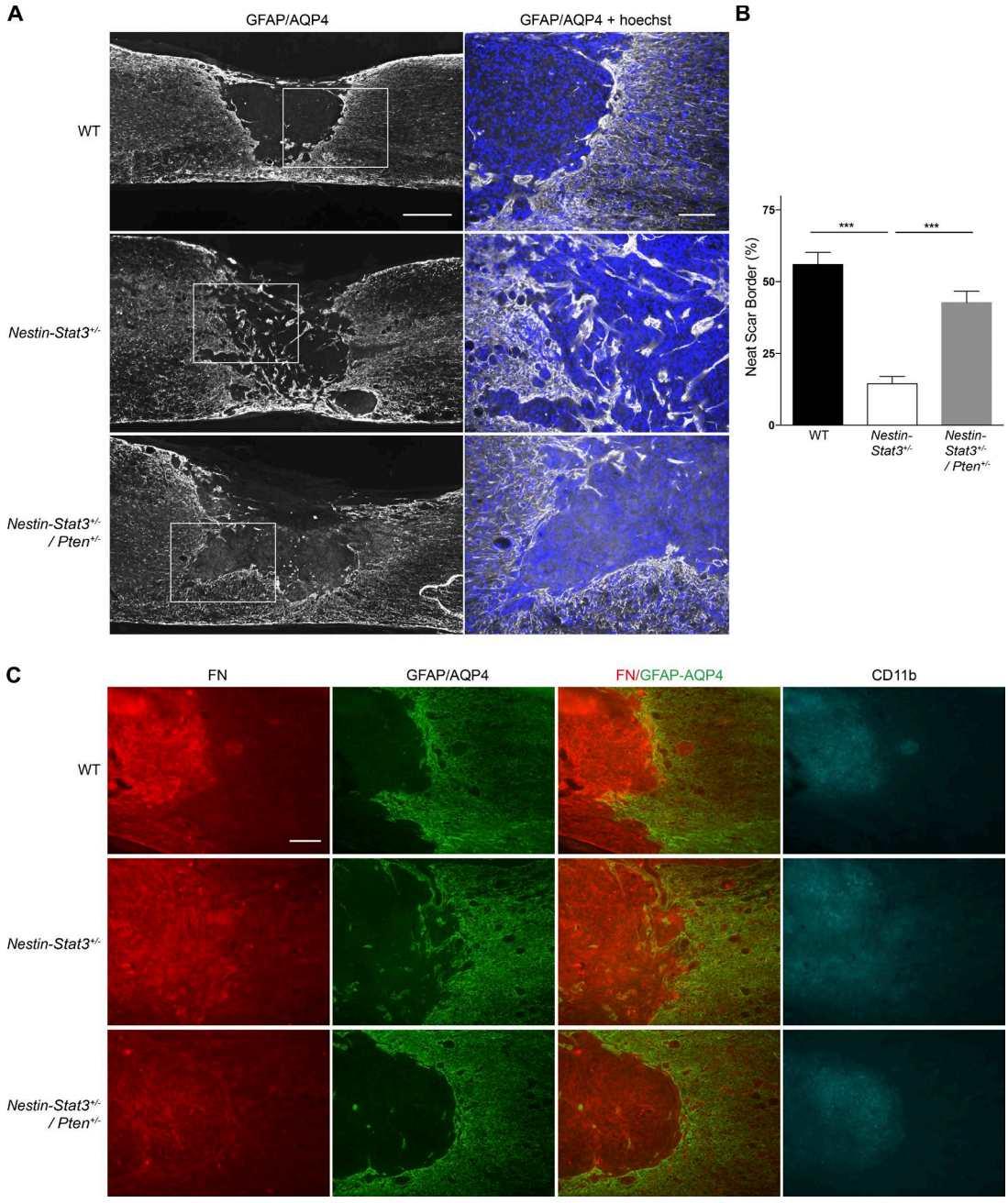

Figure 10. **Reduction of PTEN levels rescues glial scar formation in*Nestin-Stat3*$^{+/-}$ mice.** (A, left) Glial scar borders are poorly defined in *Nestin-Stat3*$^{+/-}$ mice at 21 dpi, in contrast to *Nestin-Stat3*$^{+/-}$/*Pten*$^{+/-}$ that harbor scar borders similar to WT ones. Bar, 300 µm. (Right) Higher magnification view of the insets shown on left (nuclear staining by Hoechst in blue). Bar, 100 µm. (B) Glial scar borders were scored at 21 dpi. Reduction of PTEN level in *Nestin-Stat3*$^{+/-}$ genetic background rescues the formation of glial scar borders. (C) Immunostaining for fibronectin, a fibroblast marker, or CD11b, a marker of inflammatory cells, shows an easily delineated interface between the lesion center and the reactive astrocytes in WT and *Nestin-Stat3*$^{+/-}$/*Pten*$^{+/-}$ mice, in contrast to the diffuse border in *Nestin-Stat3*$^{+/-}$ mice. Bars, 100 µm. Error bars indicate ±SEM. ***, $P < 0.001$.

gently flushing the medium with a fire-polished Pasteur pipette onto the surface of the cultures to detach cells adhering to the astrocyte monolayer. Immunostaining with anti-Iba1 antibody confirmed the purity of microglial preparations.

Bone marrow–derived macrophages were obtained as follows: femurs and tibias from adult C57BL/6J mice were dissected and crushed with a pestle. The crushed bones were washed five times in HBSS$^+$ (supplemented with 2% FBS, 10 mM Hepes, and 1% penicillin/streptomycin), and the cell suspensions were filtered through a 70-µm cell strainer (Falcon 352350; Corning) to remove debris and bone fragments and were collected by centrifugation at 280 *g* for 7 min at 4°C. The pellet was immersed in 1 ml water for 5–10 s to burst the RBCs; after which, 1 ml of 2× PBS containing 4% FBS was added, and the suspension was filtered again through a cell strainer. Pelleted cells were resuspended in DMEM/F12 supplemented with 33 mM glucose, 2 mM L-glutamine, 20 mM $NaHCO_3$, 5 mM Hepes, pH 7.4, 50 IU/ml penicillin, and 5 µg/ml streptomycin and containing 10% heat-inactivated FBS. On day 4, nonadherent cells were collected and, after centrifugation, were resuspended in fresh medium supplemented with 20% medium conditioned by L929 cells to induce their differentiation

into bone marrow–macrophages. 3 d later, immunostaining for CD11b confirmed the purity of the macrophages prepared.

Real-time quantitative PCR analyses

Total RNA was isolated from primary astrocytes using TRIzol (Invitrogen), according to the manufacturer's protocol, and was further purified with the RNeasy Mini kit (QIAGEN). Total RNA was used to synthesize cDNA with 500 ng oligo-dT primers. The cDNA synthesis was performed at 42°C for 50 min in a final volume of 20 µl using Superscript III reverse transcription (Invitrogen) followed by RNase H (Invitrogen). Real-time RT-PCR was performed using a ViiA 7 real-time PCR system (Thermo Fisher Scientific) with SYBR green (Takara Bio Inc.). In brief, the parameters were 40 cycles at annealing temperature 60°C with a hold time of 1 min, and a ramp rate of 1°C/s. The primers used are listed in Table S1. The specificity of the primers, which had been validated by the primer bank project (https://pga.mgh.harvard.edu/primerbank/), was further confirmed by examining amplification and melt curves of reactions from the astrocyte cDNA template. Analysis was performed with ViiA 7 analysis software using the automatic thresholding function, with GAPDH as an internal control. Five biological replicates per phenotype (i.e., WT versus STAT3-CKO) were run in triplicates, in at least two independent experiments.

Gelatin zymography

Gelatin zymography was performed as described previously (Xie et al., 2004). In brief, astrocytes were replated at the same density after 12 d in vitro and were then treated with 50 ng/ml TGF-α for 24 h in serum-free medium. The collected medium was further concentrated using a Centricon filter (EMD Millipore) and was then loaded into a gelatin gel that was further digested for 45 h at 37°C and was ultimately revealed using Coomassie staining.

Matrigel invasion assay

For the Matrigel invasion assay, 100 µl of Matrigel matrix (BD) at 1 mg/ml was gelled for 5 h at 37°C in trans-well inserts with 8-µm pores polyethylene terephthalate filters (BioCoat; BD). Astrocytes were trypsinized in vitro on day 13, stained with trypan blue, and counted using a hemocytometer. A total of 10^5 cells resuspended in MEM–F12 complete medium containing 1% FBS, 10 ng/ml TGF-α, and 10 µg/ml aphidicolin (Sigma-Aldrich) were allowed to migrate toward the same culture medium supplemented with 50 ng/ml TGF-α and 5 µg/ml fibronectin (Sigma-Aldrich), in the lower chamber. After 48 h at 37°C, the filters were fixed for 20 min at RT with PFA (4% in PBS, pH 7.5), and the nonmigrated cells were removed by wiping the upper side of the membranes with cotton swabs. Cell nuclei were stained using Hoechst 33258, and the filters were mounted on slides in Fluoromount medium (Diagnostic BioSystems). Using AxioVision software (ZEISS) connected to an epifluorescence microscope (Axioplan 2; ZEISS), 12 fields per membrane were captured, and the cells were counted manually. Invasion index was calculated by normalizing the counts to the WT values that were obtained within the same experiment.

Trans-well migration assays

Polyethylene terephthalate filters with 8-µm pores (BioCoat; BD) were coated with 5 µg/ml mouse laminin (Thermo Fisher Scientific) for 3 h at 37°C. Astrocytes were trypsinized on day 13 in vitro, stained with trypan blue, and counted using a hemocytometer. Astrocytes were resuspended in MEM–F12 complete medium containing 1% FBS and 10 µg/ml aphidicolin and were preincubated for 20 min in an Eppendorf tube with inhibitors before seeding 3×10^4 cells into the trans-well. The cells were allowed to migrate toward the same culture medium supplemented with 10% FBS in the lower chamber. After 15 h at 37°C, the filters were fixed for 20 min at RT with PFA (4% in PBS, pH 7.5), and the nonmigrated cells were removed by wiping the upper side of the membranes with cotton swabs. Cell nuclei were stained using Hoechst 33258, and the filters were mounted on slides in Fluoromount medium. Using AxioVision software connected to an epifluorescence microscope (Axioplan 2), 12 fields per membrane were captured, and the cells were counted manually. The migration index was calculated by normalizing the counts to control values that were obtained within the same experiment.

Analysis of α-tubulin immunoreactivity

In vitro astrocytes were replated at 14 d onto culture plates coated with 5 µg/ml laminin; 15 h later, cells were fixed with 4% PFA, and then immunostained for α-tubulin. Pictures were acquired at RT using 20× objective (Plan-Neofluar, NA 0.5) on the Axioplan-2 epifluorescence microscope (ZEISS). Cell outlines were manually traced using ImageJ software, and the mean densitometry was determined in each cell (n = 221 and 241 WT and STAT3-CKO, respectively, from 31 and 37 fields of view from three independent experiments).

Scratch-induced polarization assay

Scratch-induced polarization assay was performed as previously described in detail (Etienne-Manneville, 2006) using astrocyte monolayers prepared from WT and *Nestin-Stat3*$^{-/-}$ P1 pups.

Analysis of FA length

Primary astrocytes at 13 d in vitro were replated in normal culture medium (i.e., with 10% FBS) at low density into 8-well chambers (glass bottom; Iwaki Co.) that were previously coated with 5 µg/ml of laminin; 36 h later, cells were fixed and then immunostained for paxillin. Pictures were acquired at RT using an LSM 700 confocal microscope (ZEISS) with 63× objective (ZEISS; C-Apochromat, water immersion, 1.2 W). FA length was measured using ImageJ software (version 1.48) after manual calibration.

FA elongation

FA elongation was induced as previously described (Lee et al., 2010). In brief, astrocytes at 13 d in vitro were replated in normal culture medium (i.e., with 10% FBS) at low density into 8-well chambers (glass bottom; Iwaki) coated with 5 µg/ml of laminin. About 24 h after replating, the cells were serum starved for 14 h. Astrocytes were then treated with 10 µM LPA for 1 h in serum-free medium. In the indicated groups, SU6656 and LPA were added for the last 45 min, with final concentrations of 10 µM for both reagents. Cells were then fixed, stained, and processed as indicated in the previous section.

Analysis of FA dynamics

Primary astrocytes were transfected with RFP-CrkI (a gift from N. Mochizuki, National Cerebral and Cardiovascular Center, Osaka, Japan; Nagashima et al., 2002) on day 11 using Amaxa nucleofector (Lonza) and replated the next day into an 8-well, glass-bottom chamber (Iwaki) that was coated by 5 µg/ml laminin; 2 d later, and 2 h after a wound was made in the astrocyte monolayer using a P10 pipette tip, the fluorescent cells at the edge of the wound were recorded using a confocal microscope (LSM5, Pascal Exciter; ZEISS) that was equipped with a heat- (37°C) and gas-controlled incubation chamber (5% CO_2; Tokai Hit), which was coupled to a heated-motor stage. The objective lens (EC Plan-Neofluar, 10×, NA 0.3) was maintained at 37°C and was used to acquire a Z-stack, time-lapse series with the following parameters: zoom 4× every 15 min, seven Z-stacks (every 5 µm). Z-projections were performed with the Image Browser software (ZEISS). The formation of FA at the leading edge was tracked until disappearance using the

Manual Tracking plugin of the ImageJ software (1.48). The data were collected in six different recording sessions using three independent, primary cultures of astrocytes.

Immunoblotting

After treatment, cells were rinsed twice with ice-cold PBS, scraped into MAPK lysis buffer (50 mM Tris-HCl pH 7.5, 150 mM NaCl, 0.5% NP-40, 2 mM EDTA, 2 mM EGTA, and 2 mM sodium orthovanadate, supplemented with phosphatase inhibitor cocktails 1 and 2 (Sigma-Aldrich) and Mini Complete protease inhibitor cocktail without EDTA (Roche) on ice, passed three times through a 26-gauge needle, and then centrifuged at 13,000 *g* for 20 min at 4°C. Protein concentration was measured using a Micro BCA protein assay (Thermo Fisher Scientific), and the supernatants were mixed with sample buffer (Laemmli), boiled, and separated on polyacrylamide gels. After protein transfer to a polyvinylidene fluoride membrane (Immobilon-P; EMD Millipore), the blots were probed with the indicated primary antibodies, visualized with HRP-conjugated secondary antibodies, and developed using an enhanced chemiluminescence kit (ECL; GE Healthcare). Band intensity was quantified using an LAS-3000 imaging system (Fujifilm) and Multi Gauge software (Fujifilm).

Protein lysates from spinal cords were prepared as follows: mice were deeply anesthetized and perfused with ice-cold heparinized saline, and the spinal cords were quickly dissected and removed; 4-mm-long portions of the spinal cord from the lesion epicenter were snap-frozen in liquid nitrogen. Spinal cords were then dissociated into QIAzol lysis reagent (QIAGEN) using a sterile pilar and homogenization with P1000 micropipette (Gilson, Inc.). The proteins were then extracted using the Isogen procedure. In brief, proteins were precipitated from the organic phase using isopropanol, followed by treatment with guanidine hydrochloride and ethanol. Ultimately, the pellets were resuspended for 10 min at 55°C in SDS 1% lysis buffer containing proteases and phosphatases inhibitors. The collected supernatants were then separated by electrophoresis as described for the cellular lysates.

Gel-contraction assay

Gel-contraction assay was performed as previously described (Iwabu et al., 2004). In brief, astrocytes at 14 DIV were trypsinized and, after serial washes, were ultimately resuspended at 2×10^6 cells/ml in ice-cold, serum-free medium containing 1 mg/ml BSA. Astrocytes were then incubated with 20 µM ML-7 for 30 min on ice. Cell suspensions were then diluted 1:1 with ice-cold, neutralized collagen solution (final concentration of cell matrix collagen-type IA of 1 mg/ml), and 50 ng/ml TGF-α was added. 500 µl of this mixture (corresponding to 500,000 astrocytes) were dispensed in multiple 24-well plates and left to polymerize for 60 min at 37°C. Each matrix was then covered with 1 ml of serum-free medium containing 1 mg/ml BSA and eventually 50 ng/ml TGF-α and/or 20 µM ML-7. The compaction of the matrices was evaluated by weighting them after a 24-h incubation period at 37°C.

RhoA–GTP quantification

The activation of RhoA was assessed using two different techniques. The classical RhoA–GTP pull-down assay was performed with a kit from Thermo Fisher Scientific, with 900 µg of protein lysates for each replicate. RhoA constitutive activation in STAT3-CKO astrocytes was confirmed with an ELISA kit, according to manufacturer indications (G-Lisa assay, Cytoskeleton, Inc.); 35 µg of total proteins were used per assay. In vivo assessment of RhoA activation was performed as follows: mice were deeply anesthetized and perfused with ice-cold heparinized saline, and the spinal cords were dissected. A 4-mm-long portion of the spinal cord from the lesion epicenter was crushed using a BioMasher (Wako Pure Chemical Industries) in G-Lisa lysis buffer, according to the manufacturer's specification; sonicated twice in ice; and spun at 15,000 rpm for 5 min. The collected supernatants were distributed in vials and snap-frozen in liquid nitrogen. RhoA–GTP G-Lisa assay was performed with 50 µg of total proteins per assay. RhoA–GTP was normalized to the total RhoA expression level, which was determined by Western blotting.

Co-culture of astrocytes and leukocytes

Mouse astrocytes grown in 10% FBS were replated onto laminin on day 13 and were then gradually switched to 10% horse serum, as previously described (Wanner et al., 2013). On day 21, astrocytes and leukocytes (either microglia or bone marrow–derived macrophages. The protocol for their obtention is described in the Cell culture section) were co-cultured in 10% FBS-containing medium in the presence of the vehicle, 2 µg/ml CT04 or 2 µM H1152. On day 24, the co-cultures were fixed and stained with GFAP antibody, Alexa Fluor 488 dye–conjugated phalloidin and Texas red–conjugated-Tomato lectin (lectin from *Lycopersicon esculentum*). Images were acquired with 10× objective (Nikon Plan Apochromat, NA 0.45) using the Z-stack and tile functions of KEYENCE BZ-9000 microscope operated with a monochrome camera. BZ-II (version 1.31) analyzer software (KEYENCE) was used to obtain full-focus, tiled images.

Contusive SCI

The protocol for contusive SCI was previously described (Renault-Mihara et al., 2011). All surgical and animal-care procedures were performed in accordance with the Laboratory Animal Welfare Act and the Guide for the Care and Use of Laboratory Animals (U.S. National Institutes of Health) and were approved by the animal experimentation committee of Keio University School of Medicine (approval 13020-1). In brief, adult mice (8 wk old) were anesthetized with an i.p. injection of 100 mg/kg ketamine and 10 mg/kg xylazine. The dorsal surface of the dura mater was exposed through a laminectomy at the tenth thoracic vertebra, and SCI was induced using an Infinite Horizon Impactor (60 kilodynes; Precision Systems and Instrumentation), as previously described (Scheff et al., 2003); 1 ml of saline was s.c. injected for rehydration at the end of the procedure, and mice were kept on a 37°C warming table until awakening from anesthesia. The mice were then returned to their cages and given free access to water and food.

Wound stab injury

Adult mice (8 wk old) were anesthetized with an i.p. injection of ketamine (100 mg/kg) and xylazine (10 mg/kg). The dorsal surface of the dura mater was exposed through a laminectomy at the tenth thoracic vertebra. A 2–3-mm-long, superficial, midline incision was made along the dorsal column of the spinal cord using a surgical blade (Feather blade 11). The injured spinal cords were gently washed with saline before closing the lesion. 1 ml of saline was s.c. injected for rehydration at the end of the procedure. The mice were sacrificed 7 d after injury. Three WT and three *Nestin-Stat3*$^{-/-}$ mice were injured; one WT mouse died shortly after surgery, likely from hemorrhage before the wound stab.

Immunohistochemistry

At the indicated times after SCI, the mice were deeply anesthetized and transcardially perfused with ice-cold heparinized saline containing 50 mM NaF (Nacalai), followed by 4% PFA containing 50 mM NaF. The spinal cords were removed and immersed overnight in 4% PFA at 4°C, followed by 24 h in 10% sucrose and 24 h in 30% sucrose at 4°C. The spinal cords were then embedded in optimal cutting temperature (OCT) compound and sectioned with a cryostat (CM3050S; Leica Biosystems). 20-µm-thick, frozen sections were washed in PBS and then blocked for 30 min with a solution of PBS containing 0.4%

Triton X-100 and 1.5% FBS. Primary antibodies diluted within this solution were applied overnight at 4°C. Solutions of secondary antibodies were applied for 45 min at RT. Slides were mounted using PermaFluor mounting medium (Thermo Fisher Scientific). Negative controls for immunostaining (no primary antibodies) were systematically performed and were used for setting the microscope parameters.

Imaging

Except for live imaging, all images were acquired at RT. Fig. 7 A shows a Z-stack tile series of pictures acquired with the KEYENCE BZ-9000 microscope, processed with full focus function of the Bz-II Analyzer software. Fig. 7 B shows ZEISS LSM700 confocal microscope images (objective 40×, water immersion, C-Apochromat, 1.2 W). Fig. 8 C shows confocal imaging from a ZEISS LSM 700 microscope with a 10× objective (Plan-Apochromat, NA 0.45). Fig.8 D shows images that correspond to a single plane extracted from 1-µm step, Z-stack series, acquired using the ZEISS LSM 700 confocal microscope with a 40 × objective (water immersion, C-Apochromat, 1.2 W). Fig. 9 E shows a Z-stack tile series of images acquired with a KEYENCE BZ-9000 microscope, which were processed with the full-focus function of the Bz-II Analyzer software. Fig. 9 F shows images acquired with the ZEISS LSM700 (objective 20×, Plan-Apochromat, NA 0.8). Fig. 10 (A and D) provides images acquired with a KEYENCE BZ-9000 microscope (objective 20×, Nikon, Plan-Apochromat, NA 0.75).

miR-21 analysis

microRNAs were purified with the miRNeasy Mini kit (QIAGEN) from QIAzol lysates. Quantitative analysis was performed using a TaqMan assay 000397 for miR-21 and 001232 for normalization to snoRNA202 (Invitrogen) and either a 7900HT real-time PCR cycler (analysis in primary astrocytes) or a ViiA 7 real-time PCR system (Thermo Fisher Scientific; for spinal cord samples).

Analysis of glial scar borders

For each spinal cord analyzed, five 20-µm-thick sagittal sections were immunostained with anti-GFAP and AQP4 antibodies. Tile pictures were acquired with a KEYENCE BZ700 microscope, with 10× objective (CFI Plan Apochromat, NA 0.45). Fluorescences for GFAP (Alexa Fluor 488) and AQP4 (Alexa Fluor 555) were summed using Adobe Photoshop CC2015, as previously described (Wanner et al., 2013), to compensate for the down-regulation of GFAP in *Nestin*-STAT3$^{+/-}$ mice. For each section analyzed, 15 radial lines 300 µm long were evenly distributed along the entire perimeter of the lesion and centered on the interface (150 µm inside the lesion, 150 µm inside the tissue) and were manually traced using ImageJ software. Blind scoring of the glial scar borders at the intersection with those lines (whether a neat border or not) generated the mean score per each section (e.g., 10 neat borders of 15; i.e., 66.6%). Five mice per group (= 25 sections) were analyzed.

Statistical analysis

All analyses were performed using GraphPad Prism software version 5.00 (GraphPad Software), and all tests were two-tailed; significance is indicated as follows: *, $P < 0.05$; **, $P < 0.01$; ***, $P < 0.001$. Unless otherwise specified, values represent the means ± SEM of at least three independent experiments that were performed at least in triplicate. Replicates correspond to biological replicates, except notably, for the gel contraction assay and the trans-well migration assays, where technical replicates were made from a common cell suspension, which was obtained by pooling the cells from several culture dishes originating from multiple animals. Migration experiments were analyzed using two-way ANOVA and Bonferroni multiple comparison test. Where $n < 10$ or the data were nonnormally distributed, we used nonparametric Mann-Whitney *U* tests. Where $n \geq 10$ for normally distributed data, an unpaired *t* test or ANOVA (for more than two variables) were used for analysis. Normality of the distribution of the data was tested with d'Agostino and Pearson omnibus, Shapiro-Wilk, and Kolmogorov–Smirnov normality tests using the column statistics function of GraphPad Software.

Online supplemental material

Fig. S1 shows the expression levels of candidate molecules for the regulation of RhoA activation in STAT3-CKO astrocytes. Fig. S2 shows the corralling of bone marrow–derived macrophages by astrocytes, which relies on RhoA–ROCK pathway. Fig. S3 shows up-regulated Nestin, which identifies the lesion-proximal, reactive astrocytes after SCI. Fig. S4 describes the genetic reduction of PTEN in *Nestin-Stat3*$^{+/-}$ mice, which rescues the glial scar border formation after contusive injury. Table S1 lists the sequences of the primers used for gene expression analysis. Video 1 provides time-lapse, confocal imaging of RFP-CrkI–expressing, migrating astrocytes. Video 2 shows a confocal, 1-µm step, Z-stack series of the immunostaining for p-ERM and GFAP in the injured spinal cord of WT mice (Fig. 8 D), which is animated at 2 frames/s. Video 3 provides a confocal, 1-µm step, Z-stack series of the immunostaining for p-ERM and GFAP in the injured spinal cord of *Nestin-Stat3*$^{-/-}$ mice (Fig. 8 D), animated at 2 frames/s.

Acknowledgments

We are grateful to Drs. Tak W. Mak, Shigeyoshi Itohara, and Junichi Miyazaki for providing PTEN^{loxP}, MMP2-KO, and CAG-CAT$^{loxP/loxP}$-EGFP mice, respectively. We also thank Hiroaki Kanki, Akihiko Yoshimura, and Naoki Mochizuki for the gifts of Nestin antibody, SOCS3 antibody, and the RFP-CrkI construct, respectively. We are grateful to Tokuko Harada, Fumiko Ozawa, Shiho Nakamura, and Satoe Banno for mouse care. We thank Okano Laboratory (Shinjuku-ku, Tokyo, Japan) members, Professor Yoshiaki Toyama, and members of the SCI research group. We thank Douglas Sipp (Keio University, Shinjuku-ku, Tokyo, Japan) for invaluable comments on the manuscript.

This work was supported by fellowships from the Japan Society for Promotion of Science (P07451), as well as grants-in-aid for scientific research from Japan Society for Promotion of Science (Kakenhi grant WakateB 22700342) and Ministry of Education, Culture, Sports, Science and Technology (Kakenhi grant number WakateB 16K21360), Keio University (Sakaguchi fund), the Naito Foundation, and a medical research grant on traffic accidents from the General Insurance Association of Japan (to F. Renault-Mihara).

H. Okano is a paid scientific advisor of SanBio, Co., Ltd., and K Pharma, Inc., and M. Nakamura is a paid scientific advisor of K Pharma, Inc.

The authors declare no further competing financial interests.

Author contributions: F. Renault-Mihara conceived the study, designed and carried out the experiments, analyzed the data, and wrote the manuscript. H. Kumamaru and S. Okada characterized the different strains of Nestin reporter mice. F. Renault-Mihara, M. Mukaino, M. Shinozaki, M. Baudoux, T. Ishibashi, S. Kawabata, Y. Nishiyama, K. Sugai, and H. Kumamaru performed spinal cord injuries. S. Kawase participated in plasmid preparation. K. Yasutake performed cryostat sectioning. M. Nakamura and H. Okano supervised the study and edited the manuscript.

Submitted: 27 October 2016
Revised: 12 April 2017
Accepted: 24 May 2017

References

Anderson, M.A., J.E. Burda, Y. Ren, Y. Ao, T.M. O'Shea, R. Kawaguchi, G. Coppola, B.S. Khakh, T.J. Deming, and M.V. Sofroniew. 2016. Astrocyte scar formation aids central nervous system axon regeneration. *Nature.* 532:195–200. http://dx.doi.org/10.1038/nature17623

Betz, U.A., C.A. Vosshenrich, K. Rajewsky, and W. Müller. 1996. Bypass of lethality with mosaic mice generated by Cre-loxP-mediated recombination. *Curr. Biol.* 6:1307–1316. http://dx.doi.org/10.1016/S0960-9822(02)70717-3

Burda, J.E., A.M. Bernstein, and M.V. Sofroniew. 2016. Astrocyte roles in traumatic brain injury. *Exp. Neurol.* 275:305–315. http://dx.doi.org/10.1016/j.expneurol.2015.03.020

Bush, T.G., N. Puvanachandra, C.H. Horner, A. Polito, T. Ostenfeld, C.N. Svendsen, L. Mucke, M.H. Johnson, and M.V. Sofroniew. 1999. Leukocyte infiltration, neuronal degeneration, and neurite outgrowth after ablation of scar-forming, reactive astrocytes in adult transgenic mice. *Neuron.* 23:297–308. http://dx.doi.org/10.1016/S0896-6273(00)80781-3

Calvo, C.F., E. Amigou, C. Desaymard, and J. Glowinski. 2005. A pro- and an anti-inflammatory cytokine are synthesised in distinct brain macrophage cells during innate activation. *J. Neuroimmunol.* 170:21–30. http://dx.doi.org/10.1016/j.jneuroim.2005.08.005

Cant, S.H., and J.A. Pitcher. 2005. G protein-coupled receptor kinase 2-mediated phosphorylation of ezrin is required for G protein-coupled receptor-dependent reorganization of the actin cytoskeleton. *Mol. Biol. Cell.* 16:3088–3099. http://dx.doi.org/10.1091/mbc.E04-10-0877

Ceyzériat, K., L. Abjean, M.A. Carrillo-de Sauvage, L. Ben Haim, and C. Escartin. 2016. The complex STATes of astrocyte reactivity: How are they controlled by the JAK-STAT3 pathway? *Neuroscience.* 330:205–218. http://dx.doi.org/10.1016/j.neuroscience.2016.05.043

Chen, C.H., C.S. Sung, S.Y. Huang, C.W. Feng, H.C. Hung, S.N. Yang, N.F. Chen, M.H. Tai, Z.H. Wen, and W.F. Chen. 2016. The role of the PI3K/Akt/mTOR pathway in glial scar formation following spinal cord injury. *Exp. Neurol.* 278:27–41. http://dx.doi.org/10.1016/j.expneurol.2016.01.023

Clucas, J., and F. Valderrama. 2014. ERM proteins in cancer progression. *J. Cell Sci.* 127:267–275. http://dx.doi.org/10.1242/jcs.170027

Dey, N., H.E. Crosswell, P. De, R. Parsons, Q. Peng, J.D. Su, and D.L. Durden. 2008. The protein phosphatase activity of PTEN regulates SRC family kinases and controls glioma migration. *Cancer Res.* 68:1862–1871. http://dx.doi.org/10.1158/0008-5472.CAN-07-1182

DiMilla, P.A., K. Barbee, and D.A. Lauffenburger. 1991. Mathematical model for the effects of adhesion and mechanics on cell migration speed. *Biophys. J.* 60:15–37. http://dx.doi.org/10.1016/S0006-3495(91)82027-6

Dubreuil, C.I., M.J. Winton, and L. McKerracher. 2003. Rho activation patterns after spinal cord injury and the role of activated Rho in apoptosis in the central nervous system. *J. Cell Biol.* 162:233–243. http://dx.doi.org/10.1083/jcb.200301080

Etienne-Manneville, S. 2006. In vitro assay of primary astrocyte migration as a tool to study Rho GTPase function in cell polarization. *Methods Enzymol.* 406:565–578. http://dx.doi.org/10.1016/S0076-6879(06)06044-7

Ezratty, E.J., M.A. Partridge, and G.G. Gundersen. 2005. Microtubule-induced focal adhesion disassembly is mediated by dynamin and focal adhesion kinase. *Nat. Cell Biol.* 7:581–590. http://dx.doi.org/10.1038/ncb1262

Faulkner, J.R., J.E. Herrmann, M.J. Woo, K.E. Tansey, N.B. Doan, and M.V. Sofroniew. 2004. Reactive astrocytes protect tissue and preserve function after spinal cord injury. *J. Neurosci.* 24:2143–2155. http://dx.doi.org/10.1523/JNEUROSCI.3547-03.2004

Fujita, Y., and T. Yamashita. 2014. Axon growth inhibition by RhoA/ROCK in the central nervous system. *Front. Neurosci.* 8:338. http://dx.doi.org/10.3389/fnins.2014.00338

Goncalves, M.B., T. Malmqvist, E. Clarke, C.J. Hubens, J. Grist, C. Hobbs, D. Trigo, M. Risling, M. Angeria, P. Damberg, et al. 2015. Neuronal RARβ signaling modulates PTEN activity directly in neurons and via exosome transfer in astrocytes to prevent glial scar formation and induce spinal cord regeneration. *J. Neurosci.* 35:15731–15745. http://dx.doi.org/10.1523/JNEUROSCI.1339-15.2015

Heller, J.P., and D.A. Rusakov. 2015. Morphological plasticity of astroglia: Understanding synaptic microenvironment. *Glia.* 63:2133–2151. http://dx.doi.org/10.1002/glia.22821

Herrmann, J.E., T. Imura, B. Song, J. Qi, Y. Ao, T.K. Nguyen, R.A. Korsak, K. Takeda, S. Akira, and M.V. Sofroniew. 2008. STAT3 is a critical regulator of astrogliosis and scar formation after spinal cord injury. *J. Neurosci.* 28:7231–7243. http://dx.doi.org/10.1523/JNEUROSCI.1709-08.2008

Hoskin, V., A. Szeto, A. Ghaffari, P.A. Greer, G.P. Côté, and B.E. Elliott. 2015. Ezrin regulates focal adhesion and invadopodia dynamics by altering calpain activity to promote breast cancer cell invasion. *Mol. Biol. Cell.* 26:3464–3479. http://dx.doi.org/10.1091/mbc.E14-12-1584

Hsu, J.Y., R. McKeon, S. Goussev, Z. Werb, J.U. Lee, A. Trivedi, and L.J. Noble-Haeusslein. 2006. Matrix metalloproteinase-2 facilitates wound healing events that promote functional recovery after spinal cord injury. *J. Neurosci.* 26:9841–9850. http://dx.doi.org/10.1523/JNEUROSCI.1993-06.2006

Iliopoulos, D., S.A. Jaeger, H.A. Hirsch, M.L. Bulyk, and K. Struhl. 2010. STAT3 activation of miR-21 and miR-181b-1 via PTEN and CYLD are part of the epigenetic switch linking inflammation to cancer. *Mol. Cell.* 39:493–506. http://dx.doi.org/10.1016/j.molcel.2010.07.023

Itoh, T., T. Ikeda, H. Gomi, S. Nakao, T. Suzuki, and S. Itohara. 1997. Unaltered secretion of β-amyloid precursor protein in gelatinase A (matrix metalloproteinase 2)-deficient mice. *J. Biol. Chem.* 272:22389–22392. http://dx.doi.org/10.1074/jbc.272.36.22389

Iwabu, A., K. Smith, F.D. Allen, D.A. Lauffenburger, and A. Wells. 2004. Epidermal growth factor induces fibroblast contractility and motility via a protein kinase C δ-dependent pathway. *J. Biol. Chem.* 279:14551–14560. http://dx.doi.org/10.1074/jbc.M311981200

Johansson, C.B., C. Lothian, M. Molin, H. Okano, and U. Lendahl. 2002. Nestin enhancer requirements for expression in normal and injured adult CNS. *J. Neurosci. Res.* 69:784–794. http://dx.doi.org/10.1002/jnr.10376

John, G.R., L. Chen, M.A. Rivieccio, C.V. Melendez-Vasquez, A. Hartley, and C.F. Brosnan. 2004. Interleukin-1β induces a reactive astroglial phenotype via deactivation of the Rho GTPase-Rock axis. *J. Neurosci.* 24:2837–2845. http://dx.doi.org/10.1523/JNEUROSCI.4789-03.2004

Jones, R.J., V.G. Brunton, and M.C. Frame. 2000. Adhesion-linked kinases in cancer; emphasis on Src, focal adhesion kinase and PI 3-kinase. *Eur. J. Cancer.* 36:1595–1606. http://dx.doi.org/10.1016/S0959-8049(00)00153-2

Kawaguchi, A., T. Miyata, K. Sawamoto, N. Takashita, A. Murayama, W. Akamatsu, M. Ogawa, M. Okabe, Y. Tano, S.A. Goldman, and H. Okano. 2001. Nestin-EGFP transgenic mice: visualization of the self-renewal and multipotency of CNS stem cells. *Mol. Cell. Neurosci.* 17:259–273. http://dx.doi.org/10.1006/mcne.2000.0925

Kawamoto, S., H. Niwa, F. Tashiro, S. Sano, G. Kondoh, J. Takeda, K. Tabayashi, and J. Miyazaki. 2000. A novel reporter mouse strain that expresses enhanced green fluorescent protein upon Cre-mediated recombination. *FEBS Lett.* 470:263–268. http://dx.doi.org/10.1016/S0014-5793(00)01338-7

Khakh, B.S., and M.V. Sofroniew. 2015. Diversity of astrocyte functions and phenotypes in neural circuits. *Nat. Neurosci.* 18:942–952. http://dx.doi.org/10.1038/nn.4043

Kuo, J.C., X. Han, C.T. Hsiao, J.R. Yates III, and C.M. Waterman. 2011. Analysis of the myosin-II–responsive focal adhesion proteome reveals a role for β-pix in negative regulation of focal adhesion maturation. *Nat. Cell Biol.* 13:383–393. http://dx.doi.org/10.1038/ncb2216

Lavialle, M., G. Aumann, E. Anlauf, F. Pröls, M. Arpin, and A. Derouiche. 2011. Structural plasticity of perisynaptic astrocyte processes involves ezrin and metabotropic glutamate receptors. *Proc. Natl. Acad. Sci. USA.* 108:12915–12919. http://dx.doi.org/10.1073/pnas.1100957108

Lee, H.H., S.C. Tien, T.S. Jou, Y.C. Chang, J.G. Jhong, and Z.F. Chang. 2010. Src-dependent phosphorylation of ROCK participates in regulation of focal adhesion dynamics. *J. Cell Sci.* 123:3368–3377. http://dx.doi.org/10.1242/jcs.071555

Lima-Fernandes, E., H. Enslen, E. Camand, L. Kotelevets, C. Boularan, L. Achour, A. Benmerah, L.C. Gibson, G.S. Baillie, J.A. Pitcher, et al. 2011. Distinct functional outputs of PTEN signalling are controlled by dynamic association with β-arrestins. *EMBO J.* 30:2557–2568. http://dx.doi.org/10.1038/emboj.2011.178

Liu, K., Y. Lu, J.K. Lee, R. Samara, R. Willenberg, I. Sears-Kraxberger, A. Tedeschi, K.K. Park, D. Jin, B. Cai, et al. 2010. PTEN deletion enhances the regenerative ability of adult corticospinal neurons. *Nat. Neurosci.* 13:1075–1081. http://dx.doi.org/10.1038/nn.2603

Matsumoto, Y., M. Inden, A. Tamura, R. Hatano, S. Tsukita, and S. Asano. 2014. Ezrin mediates neuritogenesis via down-regulation of RhoA activity in cultured cortical neurons. *PLoS One.* 9:e105435. http://dx.doi.org/10.1371/journal.pone.0105435

Mierke, C.T., N. Bretz, and P. Altevogt. 2011. Contractile forces contribute to increased glycosylphosphatidylinositol-anchored receptor CD24-facilitated cancer cell invasion. *J. Biol. Chem.* 286:34858–34871. http://dx.doi.org/10.1074/jbc.M111.245183

Nagashima, K., A. Endo, H. Ogita, A. Kawana, A. Yamagishi, A. Kitabatake, M. Matsuda, and N. Mochizuki. 2002. Adaptor protein Crk is required for ephrin-B1-induced membrane ruffling and focal complex assembly of human aortic endothelial cells. *Mol. Biol. Cell.* 13:4231–4242. http://dx.doi.org/10.1091/mbc.E02-04-0181

Ng, D.C., B.H. Lin, C.P. Lim, G. Huang, T. Zhang, V. Poli, and X. Cao. 2006. Stat3 regulates microtubules by antagonizing the depolymerization activity of stathmin. *J. Cell Biol.* 172:245–257. http://dx.doi.org/10.1083/jcb.200503021

Okada, S., M. Nakamura, H. Katoh, T. Miyao, T. Shimazaki, K. Ishii, J. Yamane, A. Yoshimura, Y. Iwamoto, Y. Toyama, and H. Okano. 2006. Conditional ablation of Stat3 or Socs3 discloses a dual role for reactive astrocytes after spinal cord injury. *Nat. Med.* 12:829–834. http://dx.doi.org/10.1038/nm1425

Pannasch, U., D. Freche, G. Dallérac, G. Ghézali, C. Escartin, P. Ezan, M. Cohen-Salmon, K. Benchenane, V. Abudara, A. Dufour, et al. 2014. Connexin 30 sets synaptic strength by controlling astroglial synapse invasion. *Nat. Neurosci.* 17:549–558. http://dx.doi.org/10.1038/nn.3662

Penela, P., C. Ribas, I. Aymerich, and F. Mayor Jr. 2009. New roles of G protein-coupled receptor kinase 2 (GRK2) in cell migration. *Cell Adhes. Migr.* 3:19–23. http://dx.doi.org/10.4161/cam.3.1.7149

Renault-Mihara, F., H. Katoh, T. Ikegami, A. Iwanami, M. Mukaino, A. Yasuda, S. Nori, Y. Mabuchi, H. Tada, S. Shibata, et al. 2011. Beneficial compaction of spinal cord lesion by migrating astrocytes through glycogen synthase kinase-3 inhibition. *EMBO Mol. Med.* 3:682–696. http://dx.doi.org/10.1002/emmm.201100179

Ridley, A.J., and A. Hall. 1992. The small GTP-binding protein ρ regulates the assembly of focal adhesions and actin stress fibers in response to growth factors. *Cell.* 70:389–399. http://dx.doi.org/10.1016/0092-8674(92)90163-7

Sander, E.E., J.P. ten Klooster, S. van Delft, R.A. van der Kammen, and J.G. Collard. 1999. Rac downregulates Rho activity: reciprocal balance between both GTPases determines cellular morphology and migratory behavior. *J. Cell Biol.* 147:1009–1022. http://dx.doi.org/10.1083/jcb.147.5.1009

Sanz-Moreno, V., C. Gaggioli, M. Yeo, J. Albrengues, F. Wallberg, A. Viros, S. Hooper, R. Mitter, C.C. Féral, M. Cook, et al. 2011. ROCK and JAK1 signaling cooperate to control actomyosin contractility in tumor cells and stroma. *Cancer Cell.* 20:229–245. http://dx.doi.org/10.1016/j.ccr.2011.06.018

Scheff, S.W., A.G. Rabchevsky, I. Fugaccia, J.A. Main, and J.E. Lumpp Jr. 2003. Experimental modeling of spinal cord injury: characterization of a force-defined injury device. *J. Neurotrauma.* 20:179–193. http://dx.doi.org/10.1089/08977150360547099

Sofroniew, M.V. 2015. Astrocyte barriers to neurotoxic inflammation. *Nat. Rev. Neurosci.* 16:249–263. http://dx.doi.org/10.1038/nrn3898

Speck, O., S.C. Hughes, N.K. Noren, R.M. Kulikauskas, and R.G. Fehon. 2003. Moesin functions antagonistically to the ρ pathway to maintain epithelial integrity. *Nature.* 421:83–87. http://dx.doi.org/10.1038/nature01295

Strickland, E.R., M.A. Hook, S. Balaraman, J.R. Huie, J.W. Grau, and R.C. Miranda. 2011. MicroRNA dysregulation following spinal cord contusion: implications for neural plasticity and repair. *Neuroscience.* 186:146–160. http://dx.doi.org/10.1016/j.neuroscience.2011.03.063

Suzuki, A., M.T. Yamaguchi, T. Ohteki, T. Sasaki, T. Kaisho, Y. Kimura, R. Yoshida, A. Wakeham, T. Higuchi, M. Fukumoto, et al. 2001. T cell-specific loss of Pten leads to defects in central and peripheral tolerance. *Immunity.* 14:523–534. http://dx.doi.org/10.1016/S1074-7613(01)00134-0

Suzuki, T., H. Sakata, C. Kato, J.A. Connor, and M. Morita. 2012. Astrocyte activation and wound healing in intact-skull mouse after focal brain injury. *Eur. J. Neurosci.* 36:3653–3664. http://dx.doi.org/10.1111/j.1460-9568.2012.08280.x

Takahashi, Y., N. Carpino, J.C. Cross, M. Torres, E. Parganas, and J.N. Ihle. 2003. SOCS3: an essential regulator of LIF receptor signaling in trophoblast giant cell differentiation. *EMBO J.* 22:372–384. http://dx.doi.org/10.1093/emboj/cdg057

Teng, T.S., B. Lin, E. Manser, D.C. Ng, and X. Cao. 2009. Stat3 promotes directional cell migration by regulating Rac1 activity via its activator βPIX. *J. Cell Sci.* 122:4150–4159. http://dx.doi.org/10.1242/jcs.057109

Verma, N.K., J. Dourlat, A.M. Davies, A. Long, W.Q. Liu, C. Garbay, D. Kelleher, and Y. Volkov. 2009. STAT3-stathmin interactions control microtubule dynamics in migrating T-cells. *J. Biol. Chem.* 284:12349–12362. http://dx.doi.org/10.1074/jbc.M807761200

Voskuhl, R.R., R.S. Peterson, B. Song, Y. Ao, L.B. Morales, S. Tiwari-Woodruff, and M.V. Sofroniew. 2009. Reactive astrocytes form scar-like perivascular barriers to leukocytes during adaptive immune inflammation of the CNS. *J. Neurosci.* 29:11511–11522. http://dx.doi.org/10.1523/JNEUROSCI.1514-09.2009

Wanner, I.B., M.A. Anderson, B. Song, J. Levine, A. Fernandez, Z. Gray-Thompson, Y. Ao, and M.V. Sofroniew. 2013. Glial scar borders are formed by newly proliferated, elongated astrocytes that interact to corral inflammatory and fibrotic cells via STAT3-dependent mechanisms after spinal cord injury. *J. Neurosci.* 33:12870–12886. http://dx.doi.org/10.1523/JNEUROSCI.2121-13.2013

Wolfenson, H., A. Bershadsky, Y.I. Henis, and B. Geiger. 2011. Actomyosin-generated tension controls the molecular kinetics of focal adhesions. *J. Cell Sci.* 124:1425–1432. http://dx.doi.org/10.1242/jcs.077388

Xie, T.X., D. Wei, M. Liu, A.C. Gao, F. Ali-Osman, R. Sawaya, and S. Huang. 2004. Stat3 activation regulates the expression of matrix metalloproteinase-2 and tumor invasion and metastasis. *Oncogene.* 23:3550–3560. http://dx.doi.org/10.1038/sj.onc.1207383

Yamaguchi, M., H. Saito, M. Suzuki, and K. Mori. 2000. Visualization of neurogenesis in the central nervous system using nestin promoter-GFP transgenic mice. *Neuroreport.* 11:1991–1996. http://dx.doi.org/10.1097/00001756-200006260-00037

Zukor, K., S. Belin, C. Wang, N. Keelan, X. Wang, and Z. He. 2013. Short hairpin RNA against PTEN enhances regenerative growth of corticospinal tract axons after spinal cord injury. *J. Neurosci.* 33:15350–15361. http://dx.doi.org/10.1523/JNEUROSCI.2510-13.2013